

Covariance-based uncertainty analysis of reference equations of state

Howard Cheung,^{*,†} Jérôme Frutiger,^{*,‡} Ian H. Bell,^{*,¶} Jens Abildskov,[‡] Gürkan Sin,[‡] and Shengwei Wang[§]

[†]*Carbon Exchange (Hong Kong) Ltd., Shatin, Hong Kong*

[‡]*Process and Systems Engineering Center (PROSYS), Department of Chemical and Biochemical Engineering, Technical University of Denmark (DTU), 2800 Kgs. Lyngby, Denmark*

[¶]*Applied Chemicals and Materials Division, National Institute of Standards and Technology, Boulder, CO, 80305, USA*

[§]*Department of Building Services Engineering, The Hong Kong Polytechnic University, Hung Hom, Hong Kong*

E-mail: howard.cheung@carbonexchange.net; jfru@kt.dtu.dk; ian.bell@nist.gov

Abstract

This work presents a detailed methodology for uncertainty analysis applied to a reference equation of state (EOS) based on Helmholtz energy. With increasing interest in uncertainties of thermal process models, it is important to quantify the property uncertainties from the EOS. However, literature relating to EOS either does not report uncertainties or report underestimated values. This work addresses the issue by introducing a covariance-based methodology of uncertainty analysis based on a linear approximation. The uncertainty ranges of the EOS properties (95 % confidence intervals) are calculated from the experimental values and the EOS model structure through the parameter covariance matrix and subsequent linear error propagation. In this case study, the Helmholtz-based EOS of propane is analyzed. The uncertainty methodology is general and is applicable to any novel or existing EOS because it does not re-train the EOS. The study demonstrates the insights a thorough uncertainty analysis can give for EOS users and developers. Uncertainties vary strongly as a function of the state point, and uncertainties of saturation proper-

ties are much larger than the uncertainties of the vapor region due to the use of Maxwell criteria to calculate the saturation properties.

1 Introduction

In recent years, there have been several applications of uncertainty analysis of thermal systems. This includes the selection of working fluids for Rankine cycles,¹ virtual sensors of air conditioning systems,^{2,3} chiller control systems,⁴ and evaluation of chiller performance models for fault detection and diagnostics (FDD) algorithms.⁵ There have been systematic efforts in describing the uncertainty of both fundamental physicochemical models⁶ as well as correlation-based property models for process engineering applications.^{7,8} The uncertainties of equations of state (EOS) have not yet been adequately studied; most studies neglect the impact of the uncertainty of the EOS. On the other hand, the accuracy of the EOS is commonly considered in the literature, but analyses of accuracy only consider the difference between the output predicted by the model and experimental data. The consideration of accu-

racy instead of uncertainty is common among studies of EOS of different substances.⁹⁻¹² To this extent, the accuracy is different from the uncertainty of the output of the EOS, which is the range of statistically possible outcomes of the model given different property observations and is usually reported by the 95 % confidence interval. Uncertainty of the EOS may also be as important as the other uncertainties. For example, the accuracy of the curve fit for the saturation pressure for the refrigerant blend R410A¹³ is 0.5 % of the pressure value, and this is on par with the measurement uncertainty of refrigerant pressure.¹⁴ It is crucial, in the scope of good modeling practices, to take the uncertainties of EOS into account in order to establish the application range and the reliability of a thermal systems model.

In this manuscript a clear distinction is made between accuracy and uncertainty. The authors are aware that some studies¹³ also consider uncertainty to be the difference between modeled and measured data, and do not use the term accuracy. However, for the sake of clarity, we intend to use the term accuracy and uncertainty separately in this manuscript.

Accuracy and uncertainty are different measures and are both important to assess the performance of a model.^{15,16} Analysis of model accuracy in the literature of multiparameter reference EOS has mostly so far only involved the calculation of the closeness between some model results and known measurement values.⁹⁻¹² While a comparison of “closeness” can validate if a model yields an accurate representation of measurement values, it cannot describe the overall reliability of model results, and this model accuracy analysis does not tell the whole story for property estimates that are not associated with any known measurement values. The effect of the lack of information can only be quantified by uncertainty quantification.¹⁷ Some variables calculated by the EOS such as enthalpy and entropy can only be measured through differences relative to a reference point, and it is critical to conduct uncertainty calculations for the estimates of these variables by approaches such as covariance matrix calculation to show the variability of the estimated

enthalpy and entropy differences. Furthermore, uncertainty propagation also helps a user to understand how the uncertainty of an EOS affects the result of a thermodynamic cycle model or other process models, especially, when the operation characteristics of the cycle cannot be measured and hence an analysis of model accuracy is unavailable. To do so, it is necessary to make an analysis of the uncertainty of the EOS in addition to the commonly performed analyses on their accuracy.

Some studies^{14,18} consider the accuracy of EOS of refrigerants⁹⁻¹² as the uncertainties of EOS, and they ignore the effect of the development of the EOS to the uncertainties of EOS. Two studies were conducted to account for the uncertainty due to the covariance.^{19,20} Both of them propagated the uncertainty of measurement data that were used to fit the EOS for the uncertainty of the EOS. One of them required complete knowledge of the uncertainty of measurement data to build the EOS which is unavailable for some EOS.¹⁹ The other one only involved covariance between the input data and the EOS and did not involve covariance between the EOS parameters – a crucial part of EOS uncertainty.²⁰ In addition, the method²⁰ required re-fitting of the EOS which would be too difficult to be used for all existing EOS. Two other studies were conducted to show how to compare the propagation of the EOS parameter uncertainties to the output of a process model. The uncertainties of two EOS (cubic-type and SAFT-type) were analyzed. The method did not use the covariance matrix, but used a bootstrap method as an alternative to estimate the uncertainties of the EOS parameters.^{21,22} While the methods performed well for specific applications, it was too computationally expensive for general use. There is a need to find another method that is less computationally expensive to quantify the uncertainty of EOS of fluids.

There is also an increasing industrial interest in the analysis of the uncertainty of EOS and the state-of-the-art is to conduct the uncertainty analysis using only the accuracy of the EOS in the literature¹² or the propagation of the uncertainties from the inputs²³ for computationally efficient calculation. However, these

120 two techniques are insufficient to cover impor-
121 tant uncertainty components in the estimation
122 of a thermodynamic property of a pure sub-
123 stance as shown in Table 1.

Table 1: The steps and sources of uncertainties in the estimation of thermodynamic properties of a pure substance from an EOS

Step	Process in the task	Potential sources of uncertainties	Uncertainties propagated from previous steps	Uncertainty propagation and quantification procedures
1	Choose a model form (i.e. an EOS), a regression method and the corresponding objective function for the thermodynamic properties of a pure substance	(a) Structural uncertainty		
2	Choose the state points of the fluid at which we can measure properties and collect data to train the model	(b) Epistemic uncertainty in the choices of training data		
3	Conduct the experiments to measure the state variables such as temperature T , pressure p and density ρ for training data	(c) Stochastic and epistemic uncertainty from measurements of training data		Uncertainty analysis of the experiments for (c)
4	Perform the parameter estimation process	(d) Epistemic uncertainty of the numerical methods in the parameter estimation	(a) + (b) + (c)	Uncertainty quantification based on model covariance matrix for (a) and (b), and uncertainty propagation (e.g. through linear error propagation) for (c)
5	Obtain the input variables to EOS (e.g. temperature T and pressure p) at new conditions	(e) Subjective and stochastic uncertainties of the measurement of input variables at the new conditions	(a) + (b) + (c)	Uncertainty propagation (e.g. through linear error propagation) for (a), (b) and (c), and uncertainty analysis in the experiments for (e)
6	Evaluate the EOS to estimate the thermodynamic property of the substance at the new conditions	(f) Epistemic uncertainty of the numerical methods in the evaluation of EOS	(a) + (b) + (c) + (e)	Uncertainty propagation (e.g. through linear error propagation) for (a), (b), (c) and (e)

124 Table 1 shows the sources of uncertainties in 173
 125 the various steps to build an EOS of a pure 174
 126 substance and to use the EOS to estimate a 175
 127 thermodynamic property of the substance. It 176
 128 categorizes the uncertainty sources by struc- 177
 129 tural uncertainties, epistemic (systematic) un- 178
 130 certainties, and stochastic uncertainties accord- 179
 131 ing to Sin *et al.*²⁴ In step 1, there are structural 180
 132 uncertainties for the mathematical form of the 181
 133 EOS, because other mathematical forms could 182
 134 be used to construct the EOS. Step 2 adds epis- 183
 135 temic uncertainties to the process because the 184
 136 choices of training data of the EOS are subjek- 185
 137 tive. Step 3 adds the epistemic and stochastic 186
 138 uncertainties of experimental setups and sen- 187
 139 sors, and different training data points have 188
 140 different uncertainty values.²⁵ Step 4 only in- 189
 141 troduces epistemic uncertainties of the numer- 190
 142 ical errors of numerical methods in the param- 191
 143 eter estimation. The uncertainties involved are 192
 144 rather typically small (less than 10^{-6} % of the 193
 145 estimated dependent variable)¹⁸ and are not 194
 146 calculated. However, the same process also en- 195
 147 ables the calculation of uncertainties of param- 196
 148 eters which are highly related to the uncertain- 197
 149 ties in Steps 1 and 2. Step 5 is similar to Step 3: 198
 150 another set of data from experiments for the in- 199
 151 puts to the EOS is considered that involves the 200
 152 epistemic and stochastic uncertainties of new 201
 153 measurement values. Step 6 is the use of the 202
 154 EOS and may involve numerical iterations to 203
 155 solve implicit equations, and hence its uncer- 204
 156 tainties are not calculated. 205

157 Table 1 not only shows the sources of uncer- 206
 158 tainties but also a critical feature of the uncer- 207
 159 tainty of a model: the uncertainty of a model 208
 160 output at a condition is not only determined 209
 161 by the uncertainty of training data at that con- 210
 162 dition. While intuition suggests that the un- 211
 163 certainty of a model at an accurately measured 212
 164 training data point should be small, the uncer- 213
 165 tainty of a model output at the data point also 214
 166 depends on other factors such as the structural 215
 167 uncertainty and the subjective uncertainties in 216
 168 the choices of training data. For example, if the 217
 169 structure of the model propagates the large un- 218
 170 certainty of model outputs at some conditions 219
 171 to model outputs at other conditions, the un- 220
 172 certainty of model outputs at other conditions 221

may become larger than expected even if the
 corresponding training data points are observed
 accurately. Hence factors that affect the uncer-
 tainties of models in addition to measurement
 uncertainties of model inputs must be consid-
 ered.

While there are many important components
 of uncertainties as shown in Table 1, previously
 reported methods only cover part of them. The
 ‘‘uncertainties’’ mentioned in the work of Lem-
 mon *et al.*¹² only partially involve the calcu-
 lation of the sum of squares of errors between
 estimation and measurement values of thermo-
 dynamic properties and part of the uncertainty
 components (a) and (b) in Table 1. Uncertain-
 ties propagated by the method of Kline and Mc-
 Clintock²³ only involve uncertainty component
 (e). Some methods also fail to address issues
 such as difficulty to refit the EOS and lack of
 knowledge of measurement uncertainties of the
 training data. Hence a study should be con-
 ducted to perform the uncertainty analysis of
 EOSs with other methods.

This paper aims to describe a covariance-
 based method to calculate uncertainty due to
 both the sum of squares of residuals and the
 covariance matrix of the EOS of fluids with
 the same applicable range as the EOS, using
 the example of a multiparameter reference EOS
 of propane (CAS registry number: 74-98-6).¹²
 The developed method does not require re-
 fitting of the equation of state of the fluid and
 can be used for an EOS of any pure substance.
 The method is written in general form. If full
 and reliable measurement data are available,
 the methodology allows to take measurement
 uncertainty into account. However, if compre-
 hensive information of the uncertainty of the
 training data is not available, the methodol-
 ogy shows how the EOS prediction uncertainty
 can be calculated without measurement uncer-
 tainty. Hence, the method invites both develop-
 ers and users of EOS to consider the uncertainty
 through the covariance.

To validate the method, study its applicabil-
 ity, and illustrate its applications, the uncer-
 tainty is visualized in the saturation dome of
 the temperature-entropy and pressure-enthalpy
 diagrams. The uncertainties of sound speed,

222 specific heat, and density at different temper- 265
 223 ature and pressure are also visualized to study 266
 224 how they change under various conditions. 267

225 2 Uncertainty of parameter 270 226 estimation by parameter 271 227 covariance matrix 272

228 In this paper, the uncertainty calculation pre- 273
 229 sented is based on the parameter covariance 274
 230 matrix.^{26,27} The parameter covariance matrix 275
 231 quantifies the uncertainties of the parameters 276
 232 in an equation from a linear regression. It is 277
 233 calculated based on a linear approximation to 278
 234 a regression problem - the commonly performed 279
 235 regression for the fitting of the EOS parameters 280
 236 to experimental values - and is helpful for the 281
 237 derivation of the uncertainty of output of the 282
 238 regression equation - the equation of state. 283

239 As an example, we consider a property y that 284
 240 is described by a model $F(\mathbf{X}, \theta)$, with \mathbf{X} as the 285
 241 matrix of input variables and θ being a vec- 286
 242 tor of model parameters.²⁸ \mathbf{X} represents the 287
 243 experimental measurements. The uncertainty 288
 244 analysis is performed after the successful iden- 289
 245 tification of the best parameter estimates θ^* 290
 246 through non-linear regression (fitting to exper- 291
 247 imental values by minimization of an objective 292
 248 function) and is begun by the calculation of its 293
 249 parameter covariance matrix. 294

250 The calculation of the parameter covari- 295
 251 ance matrix allows linear error propagation 296
 252 for nonlinear regression models. Consider- 297
 253 ing the above-mentioned property y described 298
 254 by $F(\mathbf{X}, \theta)$, the underlying assumption of this 299
 255 method for uncertainty analysis is that the er- 300
 256 rors ϵ (i.e. the differences between the model 301
 257 prediction and the experiments) are indepen- 302
 258 dently distributed and defined by a Gaussian 303
 259 distribution white noise (normal distribution 304
 260 with zero mean and unit standard deviation σ) 305
 261 as expressed by Eq. (1). 306

$$262 \quad y = F(\mathbf{X}, \theta) + \epsilon \quad \epsilon \sim N(0, \sigma^2) \quad (1) \quad 263$$

264 where y is a dependent variable of a regression 307
 265 equation, \mathbf{X} is a matrix of independent variable 308
 266 of a regression equation, F is a function of a 309
 267 regression equation, θ is a parameter vector of a 310
 268 regression equation, ϵ is an error of a regression 311
 269 equation, σ is a standard deviation, $N(0, \sigma^2)$ is 312
 270 a Normal distribution with mean at zero and 313
 271 standard deviation at σ . 314

272 To calculate the parameter covariance matrix 315
 273 from the results of Eq. (1), other terms such as 316
 274 the sum of squared errors and the Jacobian of 317
 275 function $F(\mathbf{X}, \theta)$ in Eq. (1) are needed. From 318
 276 the parameter estimation, the weighted sum of 319
 277 squared errors SSE between the experimental 320
 278 and predicted data (y^{exp} and $F(\mathbf{X}, \theta)$) can be 321
 279 quantified as Eq. (2). 322

$$280 \quad SSE = \sum_i w_i \cdot (y_i^{\text{exp}} - F(\theta))^2 \quad (2) \quad 281$$

282 where SSE is the sum of squares of errors, 323
 283 exp means experimental data, and w_i is the 324
 284 weighting factor in multi-variable non-linear re- 325
 285 gression 326

287 The Jacobian of function $F(\mathbf{X}, \theta)$ represents 327
 288 the local sensitivity of the property model 328
 289 $F(\mathbf{X}, \theta)$ with respect to the parameter values 329
 290 θ . It can be calculated by taking partial deriva- 330
 291 tives of $F(\mathbf{X}, \theta)$ as shown in Eq. (3). 331

$$292 \quad J(\mathbf{X}, \theta) = \begin{bmatrix} \frac{\partial F(x_1, \theta)}{\partial \theta_1} & \cdots & \frac{\partial F(x_1, \theta)}{\partial \theta_k} & \cdots & \frac{\partial F(x_1, \theta)}{\partial \theta_m} \\ \cdots & \cdots & \cdots & \cdots & \cdots \\ \frac{\partial F(x_i, \theta)}{\partial \theta_k} & \cdots & \frac{\partial F(x_i, \theta)}{\partial \theta_k} & \cdots & \frac{\partial F(x_i, \theta)}{\partial \theta_m} \\ \cdots & \cdots & \cdots & \cdots & \cdots \\ \frac{\partial F(x_n, \theta)}{\partial \theta_1} & \cdots & \frac{\partial F(x_n, \theta)}{\partial \theta_k} & \cdots & \frac{\partial F(x_n, \theta)}{\partial \theta_m} \end{bmatrix} \quad (3) \quad 293$$

294 Its adaptation and calculation steps for EOS 332
 295 will be discussed in later sections in detail. 333
 296 The parameter w_i is the weighting factor of 334
 297 the residuals ($y_i^{\text{exp}} - F(\theta)$). When there is no 335
 298 weighting needed, w_i is assigned to be 1. In 336
 299 multivariate non-linear regression,²⁶ when fit- 337
 300 ting the experimental data of different proper- 338
 301 ties and orders of magnitude (e.g., pressure and 339
 302 temperature), a weighting factor is needed to 340
 303 normalize the residuals, and w_i will be set to 341
 304 values such as $1/(y_i^{\text{exp}})^2$. 342

305 The covariance matrix of the parameters is in 343
 306 its general form written as a function of the Ja- 344
 307 cobian matrix, $J(\mathbf{X}, \theta^*)$, and the measurement 345

301 uncertainty matrix, V :²⁶

$$COV(\theta^*) = (J(\mathbf{X}, \theta^*)^T \cdot V^{-1} \cdot J(\mathbf{X}, \theta^*))^{-1} \quad (4)$$

$J(\mathbf{X}, \theta^*)$ expresses the derivatives of $F(\mathbf{X}, \theta)$ with respect to all parameters and is evaluated at parameter estimates θ^* . V is a matrix containing the measurement uncertainty for each data point as diagonal elements. Furthermore, correlation information between the respective measurement values can be represented as off-diagonal elements. The elements of V are represented as variances σ^2 , where $\sigma_{k,k}$ would represent the standard deviation of measurement k and n the number of measured data points:

$$V = \begin{bmatrix} \sigma_{1,1}^2 & \cdots & \sigma_{1,k}^2 & \cdots & \sigma_{1,n}^2 \\ \cdots & \cdots & \cdots & \cdots & \cdots \\ \sigma_{1,k}^2 & \cdots & \sigma_{k,k}^2 & \cdots & \sigma_{k,n}^2 \\ \cdots & \cdots & \cdots & \cdots & \cdots \\ \sigma_{n,1}^2 & \cdots & \sigma_{n,k}^2 & \cdots & \sigma_{n,n}^2 \end{bmatrix} \quad (5)$$

If accurate measurement uncertainties are available, V can be used. However, correlation information is often not available for the measurement values or it is assumed that the measurements were uncorrelated. Hence, V is approximated as a diagonal matrix with measurement uncertainties:

$$V = \begin{bmatrix} \sigma_{1,1}^2 & 0 & 0 & 0 & 0 \\ 0 & \cdots & 0 & 0 & 0 \\ 0 & 0 & \sigma_{k,k}^2 & 0 & 0 \\ 0 & 0 & 0 & \cdots & 0 \\ 0 & 0 & 0 & 0 & \sigma_{n,n}^2 \end{bmatrix} \quad (6)$$

$$V = \text{diag}[\sigma_{1,1}^2, \dots, \sigma_{k,k}^2, \dots, \sigma_{n,n}^2] \quad (7)$$

302 If the measurement uncertainties are not
303 properly reported for all data points, assuming
304 arbitrary uncertainties can lead to over- or un-
305 derestimated uncertainties in θ and y . In order
306 to produce a simple assumption for the value
307 of σ^2 , which is the variance of the errors ϵ , σ^2
308 can be estimated by the sum of squared errors
309 as shown in Eq. (8).

$$\sigma^2 \approx \frac{SSE}{n - m} \quad (8)$$

310 where n is the number of data points and m is
311 the number of parameters in a regression equa-
312 tion

313 In Eq. (8), SSE is the value of the sum
314 of squared errors of the objective function ob-
315 tained from the least-squares parameter estima-
316 tion method, n is the number of data points,
317 and m is the number of parameters.

318 Hence, the covariance matrix of parameters
319 can be re-written by Eq. (9).²⁶

$$COV(\theta^*) = \sigma^2 (J(\mathbf{X}, \theta^*)^T J(\mathbf{X}, \theta^*))^{-1} \quad (9)$$

320 where COV is a covariance matrix, θ^* is an es-
321 timated parameter vector of a regression equa-
322 tion and J is a Jacobian matrix.

323 In Eq. (9), SSE is the value of the sum of
324 squared errors objective function obtained from
325 the least-squares parameter estimation method,
326 n is the number of data points, and m is the
327 number of parameters.

328 With $COV(\theta^*)$, the interdependence of the
329 parameters in the property model $F(\mathbf{X}, \theta)$ can
330 be quantified. This is done by calculating the
331 corresponding elements of the parameter corre-
332 lation matrix obtained by Eq. (10).

$$Corr(\theta_i^*, \theta_j^*) = \frac{COV(\theta_i^*, \theta_j^*)}{\sqrt{Var(\theta_i^*)Var(\theta_j^*)}} \quad (10)$$

333 where $Corr$ means correlated coefficient and
334 Var is a Variance

335 In Eq. (10), $COV(\theta_i^*, \theta_j^*)$ is the respective el-
336 ement of the covariance matrix, and $Var(\theta_i^*)$
337 and $Var(\theta_j^*)$ are the variances of the respective
338 parameters.

339 The covariance matrix of the property model
340 predictions can be approximated by linear error
341 propagation through the Jacobian of a vector of
342 independent variables \vec{x} and the covariance of
343 the parameter estimates as shown in Eq. (11).

$$COV(y^{\text{pred}}) = J(\vec{x}, \theta^*) COV(\theta^*) J(\vec{x}, \theta^*)^T \quad (11)$$

344 where pred means predicted values.
With the covariance matrices of the param-

eters and the property model predictions, the uncertainty of the parameters and the property model predictions can be quantified using the confidence intervals of the parameters and property model predictions. If the assumptions behind the model are satisfied (as assumed in the previous steps), the parameter estimates will follow a Student t -distribution and the confidence interval of parameters can be expressed as Eq. (12).

$$\theta_{1-\gamma_t/2}^* = \theta^* \pm \sqrt{\text{diag}(\text{COV}(\theta^*))} \cdot t(n-m, \gamma_t/2) \quad (12)$$

where γ_t is the Student t distribution percentile and diag is a vector formed by the diagonal entries of a matrix.

Similarly, the confidence intervals of the property predictions are given by Eq. (13).

$$y_{1-\gamma_t/2}^{\text{pred}} - y^{\text{pred}} = \pm \sqrt{\text{diag}(\text{COV}(y^{\text{pred}}))} \cdot t(n-m, \gamma_t/2) \quad (13)$$

In Eqs. (12) and (13), $t(n-m, \gamma_t/2)$ is the Student t -distribution value corresponding to the $\gamma_t/2$ percentile of the Student t -distribution, $\text{diag}(\text{COV}(\theta^*))$ represents the diagonal elements of $\text{COV}(\theta^*)$, and $\text{diag}(\text{COV}(y^{\text{pred}}))$ are the corresponding diagonal elements of $\text{COV}(y^{\text{pred}})$.

The confidence intervals from Eqs. (12) and (13) can be regarded as the uncertainty of the parameters and the property model predictions, respectively, in very simple regression models with uncorrelated parameters. They quantify the range of possible outcomes of the EOS if the regression process is repeated with data points obtained at other experimental conditions. However, since all parameters are correlated with each other at some degree, the basic theory is too simple for complex models like EOS which estimate different types of outputs based upon various types of experimental data. The forthcoming sections describe how the theory can be applied to the EOS to calculate its uncertainty.

The authors would also like to highlight the problem of systematic measurement errors. The assumption of ideally and independently

distributed measurement errors (according to Eq. (1)) would correspond to completely uncorrelated measurement data (white noise). However, it is likely that data points from the same data source will be correlated and systematically higher or lower than another source. These systematic errors depend on many factors such as the experimental set-up, the location and the experimentalists themselves. In the current methodology these correlated measurement errors have not been systematically incorporated, since it is out of the scope of the current work.

3 Equation of state and its uncertainty calculation

The thermodynamic properties of pure fluids were first calculated by using the ideal gas laws and variations of ideal gas laws.^{29,30} In recent years, EOS have been developed that are based on the fundamental formulation of the non-dimensionalized Helmholtz energy $\alpha = a/(RT)$ with temperature T and density ρ as independent variables. Extensive literature is available on these highly flexible empirical multiparameter equations of state.^{9,12,30} The detailed formulations and derivations for the equations of state used in this paper can be found in the supporting material, where all the property equations and variables of the EOS are listed.

3.1 Uncertainty of properties with T and ρ as inputs

We use the following formulation of the non-dimensionalized Helmholtz energy α with temperature and density as independent variables:

$$\alpha([\theta_{\text{EOS}}, T_c, \rho_c], T, \rho) = \alpha^0([\theta_{\text{EOS}}, T_c, \rho_c], T, \rho) + \alpha^f([\theta_{\text{EOS}}, T_c, \rho_c], T, \rho) \quad (14)$$

where α is dimensionless Helmholtz energy, α^0 is ideal gas component of dimensionless Helmholtz energy, α^f is dimensionless Helmholtz energy due to intermolecular forces,

414 δ , is reduced density, τ is reciprocal of reduced 463
 415 temperature and EOS means equation of state. 464

416 Equation (14) is the the sum of two terms: α^0 465
 417 is the non-dimensionalized Helmholtz energy of 466
 418 an ideal gas, and α^f accounts for the contri- 467
 419 bution to Helmholtz energy as a result of inter- 468
 420 molecular forces, where θ_{EOS} are the parameters 469
 421 of the EOS. We use the notation $[\theta_{\text{EOS}}, T_c, \rho_c]$ 470
 422 to clearly indicate that θ_{EOS} , T_c and ρ_c are 471
 423 model parameters of the EOS. ρ_c is the density 472
 424 at the critical point and T_c the critical tempera- 473
 425 ture. In some EOS (one example would be that 474
 426 of refrigerant R-134a³¹), a reference state other 475
 427 than the critical point is used to reduce the 476
 428 temperature and density, but that is not fur- 477
 429 ther discussed here. In this work, we consider
 430 the EOS of propane of Lemmon *et al.*¹² and
 431 the EOS parameters θ_{EOS} can be obtained from
 432 the same work. From the non-dimensionalized
 433 Helmholtz energy EOS other fluid properties
 434 can be derived and calculated given tempera-
 435 ture T , density ρ and parameters $[\theta_{\text{EOS}}, T_c, \rho_c]$:
 436 the pressure p , the molar internal energy u , the
 437 molar enthalpy h , the molar entropy s , the mo-
 438 lar Gibbs energy g , the molar Helmholtz energy
 439 a , the molar isochoric heat capacity c_v , the mo-
 440 lar isobaric heat capacity c_p , the speed of sound
 441 w , the fugacity coefficient ϕ , the second virial 478
 442 coefficient B , the third virial coefficient C , and 479
 443 the ideal gas isobaric heat capacity c_{p0} ^{12,30} (see 480
 444 ?? for detailed derivations of all property equa- 481
 445 tions). 482

446 where p , Pressure in Pa, ρ is density in 483
 447 mol/m³, ρ_c is critical density in mol/m³, u , is 484
 448 molar internal energy in J/mol, h is molar en- 485
 449 thalpy in J/mol, s is molar entropy in J/mol- 486
 450 K, g is molar Gibbs energy in J/mol-K, a is 487
 451 molar Helmholtz energy in J/mol, c_v is molar 488
 452 isochoric heat capacity in J/mol-K, c_p is molar 489
 453 isobaric heat capacity in J/mol-K, w is speed 490
 454 of sound in m/s, ϕ is Fugacity coefficient, B is 491
 455 second virial coefficient in m³/mol, C is third 492
 456 virial coefficient in m⁶/mol, c_{p0} is ideal gas spe- 493
 457 cific isobaric heat capacity in J/mol-K. 494

458 In the literature, Eq. (14) is conventionally 495
 459 written in terms of the reduced density $\delta = \rho/\rho_c$ 496
 460 and reciprocal reduced temperature $\tau = T_c/T$, 497
 461 where δ and τ are the independent variables of 498
 462 the EOS and θ_{EOS} are the parameters. How- 499

ever, there are usually considerable differences
 among investigators in the measurement of the
 critical temperature T_c and critical density ρ_c as
 shown by Lemmon *et al.*¹² This means that it is
 necessary to take into account the measurement
 uncertainties of the critical point when calculat-
 ing the uncertainty of the EOS outputs.

The covariance-based uncertainty analysis
 method, which version for simple linear regres-
 sion models has been outlined in Section 2, is
 now described for the Helmholtz-based EOS.
 Equation (14) can be written analogously to
 Eq. (1) assuming ideally and independently dis-
 tributed errors defined by a Gaussian distribu-
 tion white noise.

$$y = F(\mathbf{X}, \vartheta) + \epsilon \quad \epsilon \sim N(0, \sigma^2) \quad (15)$$

$$\mathbf{y} := [p, u, h, s, g, a, c_v, c_p, \omega, \phi, B, C, c_{p0}] \quad (16)$$

$$\mathbf{X} := (T, \rho) \quad (17)$$

$$\vartheta := [\theta_{\text{EOS}}, T_c, \rho_c] \quad (18)$$

T_c and ρ_c are defined according to the ex-
 perimental results of thermodynamic properties
 around the critical point, and we assume that
 the parameter estimation for θ_{EOS} (parameter
 optimization and fitting to a large set of exper-
 imental data) has been completed by the devel-
 opers of the EOS . The set of parameters called
 θ_{EOS}^* is known from the literature.¹¹ Hence, the
 parameter estimates θ_{EOS}^* are used in this study
 for the uncertainty analysis and re-training of
 the data is not necessary.

The parameters of the EOS are given by
 $\theta_{\text{EOS}} = [\theta_1, \dots, \theta_j, \dots, \theta_m]$, with m being the num-
 ber of parameters.

However, experimental data need to be col-
 lected or taken from the work of the developers
 of the EOS because it is needed to calculate the
 errors (differences between experimental data
 and predicted values by the EOS). For exam-
 ple, in the case of propane, the EOS has been
 fitted to experimental data of p , p_{sat} , c_v , c_p , w ,
 B , c_{p0} as functions of T and ρ . These vari-

ables are called fitted (or observed) variables because some of their values are measured and included in the fitting process. Other variables (e.g., u , h , s , g , a , C and ϕ) are called (purely) predicted variables because none of their experimental measurements are included in the fitting process of the EOS. Some EOSs may have different sets of fitted variables and predicted variables depending on experimental data availability, but the proposed method focuses on using the aforementioned set of fitted and predictive variables for simplicity. The parameter covariance matrix (i.e. the uncertainty information of the parameter estimates θ_{EOS}^*) is obtained through the use of data. The uncertainties of T , ρ , p , c_v , c_p , w , B and c_{p0} as well as u , h , s , C , ϕ , a and g estimated by the EOS are then obtained by linear error propagation.

For the fitted properties, there are a number of n experimental data points respectively, e.g. $p^{\text{exp}} = [p_1^{\text{exp}}, \dots, p_{n_p}^{\text{exp}}]$, $c_v^{\text{exp}} = [c_{v1}^{\text{exp}}, \dots, c_{v_{n_{c_v}}}^{\text{exp}}]$, etc.

We describe specifically how the uncertainty analysis described in Section 2 can be applied to the estimation of the uncertainty of the predictions of EOS. We will use the notation introduced above for $\alpha([\theta_{\text{EOS}}, T_c, \rho_c], T, \rho)$, where the parameters for the EOS are θ_{EOS} , T_c and ρ_c , and the independent variables are T and ρ .

Equation (9) described the covariance matrix of the parameters determined from the variances of errors σ^2 and the Jacobian $J(\theta^*)$, where σ^2 is obtained from the sum of squared errors SSE of the objective function from the least-square parameter estimation. Hence, in the case of the fundamental EOS for propane, as described by Lemmon *et al.*,¹² SSE is described as the sum of squared relative errors – the difference between the predicted and experimental property value divided by the experimental value (least square regression). Hence, for the example of the fitted property c_p , its variance σ^2 should be written as

$$\sigma_{c_p}^2 \approx \frac{SSE_{c_p}}{n_{c_p} - m_{c_p}} \quad (19)$$

where n_{c_p} is the number of data points for c_p and m_{c_p} is the number of EOS parameters that are needed to calculate c_p using the EOS (note $n_{c_p} - m_{c_p} > 0$). SSE_{c_p} is the value of the sum of

squared relative errors objective function from the parameter estimation.¹² In order to obtain SSE_{c_p} the parameter estimation does not need to be retrained:

$$SSE_{c_p} = \sum_{i=1}^{n_{c_p}} \left[\frac{c_{p_i}^{\text{exp}} - c_p(\theta_{\text{EOS}}^*, \tau_i, \delta_i)}{c_{p_i}^{\text{exp}}} \right]^2 \quad (20)$$

where i is the index for the experimental condition (T_i , ρ_i), $c_{p_i}^{\text{exp}}$ is the experimental value of specific heat and $c_p(\theta_{\text{EOS}}^*, \tau_i, \delta_i)$ is the predicted specific heat value. The estimates for variances of the other fitted properties are obtained for $\sigma_{c_v}^2$, σ_w^2 , σ_B^2 , $\sigma_{c_{p0}}^2$ and $\sigma_{p_c}^2$. The estimate for the error of T_c and ρ_c ($\sigma_{T_c}^2$ and $\sigma_{\rho_c}^2$) can be calculated from the standard deviation of the experimental measurements. Lemmon *et al.*¹² used a different objective function for the residual errors in the pressure as shown in Eq. (21), in order to obtain similar magnitudes of the liquid and vapor phase.

$$SSE_p = \sum_i \left[\frac{p_i^{\text{exp}} - p(\theta_{\text{EOS}}^*, \tau_i, \delta_i)}{\rho_i^{\text{exp}} \left(\frac{\partial p_i}{\partial \rho_i} \right)_T} \right]^2 \quad (21)$$

where p_i^{exp} is the experimental pressure value, $p(\theta_{\text{EOS}}^*, \tau_i, \delta_i)$ is the predicted pressure value, ρ_i^{exp} is the experimental density value and $\left. \frac{\partial p_i}{\partial \rho_i} \right|_T$ is the partial derivative of the pressure with respect to the density calculated at θ_{EOS}^* .

In order for the uncertainty assessment of the EOS to be consistent with the EOS itself, the exact objective function used in the training of the EOS is needed, but this is very difficult to achieve in practice. The state-of-the-art fitting process includes addition and removal of data points and constraints in an iterative fashion, and it is not possible to obtain the weights that were ultimately used in the regression process. Therefore, the weights that were used in the fitting process of Lemmon *et al.*¹² are unknowable, and an estimation of the objective function (i.e. the corresponding SSE) is required.

While Eq. (21) is appropriate for pressure data points with density and temperature as

575 independent variables, it is not suitable for va- 608
 576 por pressure data. For vapor pressure data, the 609
 577 desired residue would be

$$SSE_{p_{\text{sat}}} = \sum_i \left[\frac{p_i^{\text{exp}} - p_{\text{sat}}(\theta_{\text{EOS}}^*, \tau_i)}{p_i^{\text{exp}}} \right]^2, \quad (22)$$

578 though this form is not suitable because the 616
 579 evaluation of p^{sat} requires an iterative solution 617
 580 for the vapor pressure, which is a calculation 618
 581 fraught with potential perils. For that reason, 619
 582 it is preferable, and common practice, to mini- 620
 583 mize the difference in Gibbs energy between the 621
 584 saturated liquid and vapor phases for the given 622
 585 temperature and pressure (see for instance Bell 623
 586 et al.³²). In this case, the densities must be 624
 587 solved for in each phase, but the full resolution 625
 588 of the Maxwell criteria is not required.

589 To describe the minimization process in terms 608
 590 of SSE , Eq. (23) is used with vapor pressure 609
 591 data.

$$SSE_g = \sum_i \left[\frac{g(\theta_{\text{EOS}}^*, \tau_i, \frac{\rho_{\text{min},i}}{\rho_c}) - g(\theta_{\text{EOS}}^*, \tau_i, \frac{\rho_{\text{max},i}}{\rho_c})}{RT_i^{\text{exp}}} \right]^2 \quad (23)$$

$$\rho_{\text{min},i} = \min(\bar{\rho}(T_i^{\text{exp}}, p_i^{\text{exp}})) \quad (24)$$

$$\rho_{\text{max},i} = \max(\bar{\rho}(T_i^{\text{exp}}, p_i^{\text{exp}})) \quad (25)$$

592 where ρ_{min} is the minimum density calculated 608
 593 by iteratively solving for density from the speci- 609
 594 fied temperature and pressure, ρ_{max} is the maxi- 610
 595 mum density calculated from the same iterative 611
 596 calculation of density, R is the universal gas 612
 597 constant, T_i^{exp} is the experimental temperature 613
 598 reading in the vapor pressure data. 614

599 One may wonder if the SSE in Eq. (23) is 608
 600 suitable to describe the deviation in pressure 609
 601 differences between estimated and measured va- 610
 602 por pressure. To verify that Eq. (23) is approxi- 611
 603 mately equivalent to Eq. (22), the relative devi- 612
 604 ation between the estimated and pressure pres- 613
 605 sure is plotted with the difference of the Gibbs 614
 606 energy of saturated liquid and vapor divided by 615
 607 the product of the gas constant and T , as well 616

608 as more accurate approximations to Eq. (22). 609
 610 The derivations in the supplemental material 611
 612 explain how this non-dimensionalization can be 613
 614 obtained, following the assumptions that a) 615
 616 a first-order series expansion of Gibbs energy 617
 618 with respect to pressure difference can be used, 619
 620 b) the vapor phase derivative of Gibbs energy 621
 622 with respect to pressure at constant tempera- 623
 624 ture is much greater in magnitude than that of 624
 625 the liquid phase, and c) the vapor phase can be 625
 treated as an ideal gas.

Figure 1 presents numerical values for each 608
 of the approximations to the vapor pressure 609
 residue of propane. This figure demonstrates 610
 that $\Delta g/(RT)$ provides a fair representation 611
 of the saturation pressure residue although the 612
 second-order expansion yields a superior evalu- 613
 ation of the vapor pressure residue. 614

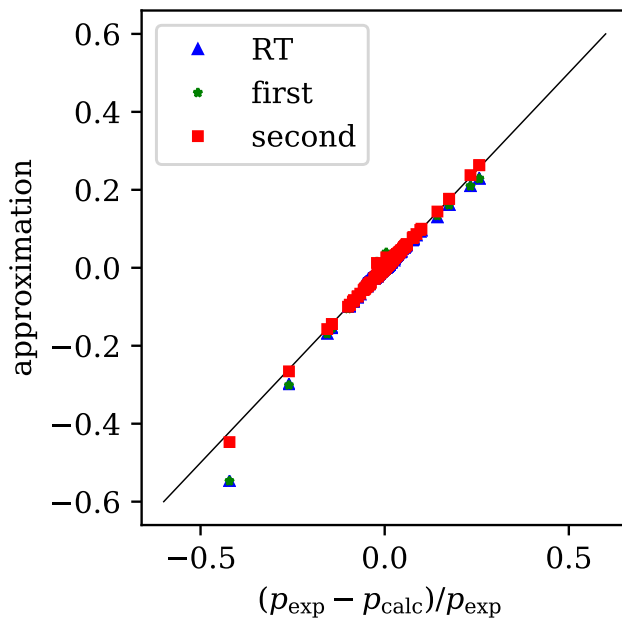


Figure 1: Comparing three different approxima- 608
 tions to the deviation in pressure with relative 609
 error in pressure calculation. For more infor- 610
 mation, see the derivations in the supplemental 611
 material (RT: $res = \Delta g/(RT)$, first: a first- 612
 order expansion in pressure difference, dropping 613
 the liquid derivative without any further simpli- 614
 fications, second: a second order expansion in 615
 pressure difference without any further simpli- 616
 fications)

The results show that the difference of Gibbs 608
 energy can effectively describe the difference 609

628 between estimated and measured vapor pres- 677
 629 sure. However, since the differences of pressure 678
 630 are not really used in the estimation of the co- 679
 631 efficients in the Helmholtz-energy-based EOS, 680
 632 Eq. (23) is used in this study. 681

633 A diagonal matrix containing all the er- 682
 634 ror variances can then be built as follows in 683
 635 Eq. (26). 684

636 where V is a matrix of variance. 685

637 The V matrix in Eq. (26) contain $2n_{p_v}$ num- 686
 638 ber of σ_g^2 because each σ_g^2 is calculated by two 687
 639 predicted values: the predicted values of Gibbs 688
 640 energy of saturated vapor and the predicted val- 689
 641 ues of Gibbs energy of saturated liquid. 690

642 The Jacobian for all of the fitted properties 691
 643 needs to be calculated at the specific experi- 692
 644 mental measurement point of the variables T 693
 645 and ρ (or τ and δ respectively for their dimen- 694
 646 sionless form), and at the specific fitted param- 695
 647 eter values θ_{EOS}^* . However, since the variances
 648 σ_p^2 , σ_g^2 , $\sigma_{c_p}^2$, $\sigma_{c_v}^2$, σ_w^2 , σ_B^2 , $\sigma_{c_{p0}}^2$, $\sigma_{T_c}^2$ and $\sigma_{p_c}^2$ used
 649 relative errors, the elements of the Jacobians
 650 need to be normalized by their corresponding
 651 experimental value. As an example, the gen-
 652 eral analytical expression of the Jacobian of p
 653 can be written as Eq. (27).

654 While the Jacobians of an experimental data
 655 point of most fitted variables can be calculated
 656 in a similar way as Eq. (27), the Jacobian of
 657 each experimental observation of vapor pressure
 658 are calculated differently because they have two
 659 predicted values of Gibbs energy in each dif-
 660 ference term in Eq. (23). To involve the par-
 661 tial derivatives of both predicted values in the
 662 SSE_g , the Jacobian of vapor pressure is a $2 \times$
 663 $(m+2)$ matrix as Eq. (28)

664 The first row of the Jacobian in Eq. (28) cor-
 665 responds to the predicted values of Gibbs en-
 666 ergy of the maximum density value at the vapor
 667 pressure, and the second row of the Jacobian
 668 corresponds to the predicted values of Gibbs
 669 energy of the minimum density values at the
 670 corresponding temperature.

671 The Jacobian of the fitted data of p at multi-
 672 ple experimental data points of τ and δ , evalu-
 673 ated at the parameter estimates θ_{EOS}^* is then
 674 given by Eq. (29), where $J_p(\theta_{\text{EOS}}^*, \tau, \delta)$ is a 696
 675 $n_p \times (m+2)$ matrix with $\theta_{\text{EOS}}^* = [\theta_1^*, \dots, \theta_m^*]$, 697
 676 $\tau = [\tau_1, \dots, \tau_{n_p}]$ and $\delta = [\delta_1, \dots, \delta_{n_p}]$. p_i^{exp} are 698

the corresponding experimental values used to
 normalize the Jacobian. The method to calcu-
 late the partial derivatives is discussed in the
 Supplementary Materials for reference.

Assuming that the uncertainties of critical
 properties have no effect on the estimation
 of the coefficients θ_{EOS} and do not propagate
 through their estimation process, the Jacobian
 of p evaluated at the experimental values can
 be simplified by setting the last two columns of
 values in Eq. (29) as zeros.

It is important to notice that J_p is evaluated
 at the parameter estimates θ_{EOS}^* , but is a func-
 tion of T and ρ . In analogy, the Jacobian for
 the other fitted data can be obtained, giving
 J_{c_v} , J_{c_p} , J_w , J_B and $J_{c_{p0}}$. Since we are account-
 ing for the effect of the uncertainties of critical
 densities and critical temperature, their Jaco-
 bians are given as

$$\begin{aligned}
 J_{T_c} &= \begin{bmatrix} 0_{1 \times m} & \frac{\partial T_c}{\partial T_{c,1}} \frac{1}{T_{c,1}} & 0 \\ \dots & \dots & \dots \\ 0_{1 \times m} & \frac{\partial T_c}{\partial T_{c,i}} \frac{1}{T_{c,i}} & 0 \\ \dots & \dots & \dots \\ 0_{1 \times m} & \frac{\partial T_c}{\partial T_{c,n_{T_c}}} \frac{1}{T_{c,n_{T_c}}} & 0 \end{bmatrix} \\
 &= \begin{bmatrix} 0_{1 \times m} & \frac{1}{n_{T_c} T_{c,1}} & 0 \\ \dots & \dots & \dots \\ 0_{1 \times m} & \frac{1}{n_{T_c} T_{c,i}} & 0 \\ \dots & \dots & \dots \\ 0_{1 \times m} & \frac{1}{n_{T_c} T_{c,n_{T_c}}} & 0 \end{bmatrix} \quad (30)
 \end{aligned}$$

$$\begin{aligned}
 J_{\rho_c} &= \begin{bmatrix} 0_{1 \times m} & 0 & \frac{\partial \rho_c}{\partial \rho_{c,1}} \frac{1}{\rho_{c,1}} \\ \dots & \dots & \dots \\ 0_{1 \times m} & 0 & \frac{\partial \rho_c}{\partial \rho_{c,i}} \frac{1}{\rho_{c,i}} \\ \dots & \dots & \dots \\ 0_{1 \times m} & 0 & \frac{\partial \rho_c}{\partial \rho_{c,n_{\rho_c}}} \frac{1}{\rho_{c,n_{\rho_c}}} \end{bmatrix} \\
 &= \begin{bmatrix} 0_{1 \times m} & 0 & \frac{1}{n_{\rho_c} \rho_{c,1}} \\ \dots & \dots & \dots \\ 0_{1 \times m} & 0 & \frac{1}{n_{\rho_c} \rho_{c,i}} \\ \dots & \dots & \dots \\ 0_{1 \times m} & 0 & \frac{1}{n_{\rho_c} \rho_{c,n_{\rho_c}}} \end{bmatrix} \cdot \quad (31)
 \end{aligned}$$

The combined Jacobian of the fitted data p ,
 p_v , c_v , c_p , w , B and c_{p0} can constructed as in
 Eq. (32).

$$V = \text{diag}[\underbrace{\sigma_p^2, \dots, \sigma_p^2}_{n_p}, \underbrace{\sigma_g^2, \dots, \sigma_g^2}_{2n_{p_v}}, \underbrace{\sigma_{c_v}^2, \dots, \sigma_{c_v}^2}_{n_{c_v}}, \underbrace{\sigma_{c_p}^2, \dots, \sigma_{c_p}^2}_{n_{c_p}}, \underbrace{\sigma_w^2, \dots, \sigma_w^2}_{n_w}, \underbrace{\sigma_B^2, \dots, \sigma_B^2}_{n_B}, \underbrace{\sigma_{n_{c_{p0}}}^2, \dots, \sigma_{n_{c_{p0}}}^2}_{n_{c_{p0}}}, \underbrace{\sigma_{T_c}^2, \dots, \sigma_{T_c}^2}_{n_{T_c}}, \underbrace{\sigma_{\rho_c}^2, \dots, \sigma_{\rho_c}^2}_{n_{\rho_c}}] \quad (26)$$

$$J_p([\theta_{\text{EOS}}^*, T_c, \rho_c], T_i, \rho_i) = \frac{1}{p_i^{\text{exp}}} \left[\frac{\partial p}{\partial \theta_1}(\theta_{\text{EOS}}^*, T_i, \rho_i) \quad \dots \quad \frac{\partial p}{\partial \theta_M}(\theta_{\text{EOS}}^*, T_i, \rho_i) \quad \frac{\partial p}{\partial T_c}(\theta_{\text{EOS}}^*, T_i, \rho_i) \quad \frac{\partial p}{\partial \rho_c}(\theta_{\text{EOS}}^*, T_i, \rho_i) \right] \quad (27)$$

$$J_{p_v}([\theta_{\text{EOS}}^*, T_c, \rho_c], T_i, p_i) = \frac{1}{RT_i} \times \left[\begin{array}{cccc} \frac{\partial g}{\partial \theta_1}(\theta_{\text{EOS}}^*, T_i, \rho_{\text{min},i}) & \dots & \frac{\partial g}{\partial \theta_M}(\theta_{\text{EOS}}^*, T_i, \rho_{\text{min},i}) & \frac{\partial g}{\partial T_c}(\theta_{\text{EOS}}^*, T_i, \rho_{\text{min},i}) & \frac{\partial g}{\partial \rho_c}(\theta_{\text{EOS}}^*, T_i, \rho_{\text{min},i}) \\ \frac{\partial g}{\partial \theta_1}(\theta_{\text{EOS}}^*, T_i, \rho_{\text{max},i}) & \dots & \frac{\partial g}{\partial \theta_M}(\theta_{\text{EOS}}^*, T_i, \rho_{\text{max},i}) & \frac{\partial g}{\partial T_c}(\theta_{\text{EOS}}^*, T_i, \rho_{\text{max},i}) & \frac{\partial g}{\partial \rho_c}(\theta_{\text{EOS}}^*, T_i, \rho_{\text{max},i}) \end{array} \right] \quad (28)$$

$$J_p = \left[\begin{array}{cccc} \frac{\partial p}{\partial \theta_1} \Big|_{\theta_{\text{EOS}}^*, T_1, \rho_1}^{\text{exp}} & \dots & \frac{\partial p}{\partial \theta_m} \Big|_{\theta_{\text{EOS}}^*, T_1, \rho_1}^{\text{exp}} & \frac{\partial p}{\partial T_c} \Big|_{\theta_{\text{EOS}}^*, T_1, \rho_1}^{\text{exp}} \frac{\partial \tau_1}{\partial T_c} & \frac{\partial p}{\partial \delta_1} \Big|_{\theta_{\text{EOS}}^*, T_1, \rho_1}^{\text{exp}} \frac{\partial \delta_1}{\partial \rho_c} \\ p_1 & \dots & p_1 & p_1 & p_1 \\ \dots & \dots & \dots & \dots & \dots \\ \frac{\partial p}{\partial \theta_1} \Big|_{\theta_{\text{EOS}}^*, T_i, \rho_i}^{\text{exp}} & \dots & \frac{\partial p}{\partial \theta_m} \Big|_{\theta_{\text{EOS}}^*, T_i, \rho_i}^{\text{exp}} & \frac{\partial p}{\partial T_c} \Big|_{\theta_{\text{EOS}}^*, T_i, \rho_i}^{\text{exp}} \frac{\partial \tau_i}{\partial T_c} & \frac{\partial p}{\partial \delta_i} \Big|_{\theta_{\text{EOS}}^*, T_i, \rho_i}^{\text{exp}} \frac{\partial \delta_i}{\partial \rho_c} \\ p_i & \dots & p_i & p_i & p_i \\ \dots & \dots & \dots & \dots & \dots \\ \frac{\partial p}{\partial \theta_1} \Big|_{\theta_{\text{EOS}}^*, T_{n_p}, \rho_{n_p}}^{\text{exp}} & \dots & \frac{\partial p}{\partial \theta_m} \Big|_{\theta_{\text{EOS}}^*, T_{n_p}, \rho_{n_p}}^{\text{exp}} & \frac{\partial p}{\partial T_c} \Big|_{\theta_{\text{EOS}}^*, T_{n_p}, \rho_{n_p}}^{\text{exp}} \frac{\partial \tau_{n_p}}{\partial T_c} & \frac{\partial p}{\partial \delta_{n_p}} \Big|_{\theta_{\text{EOS}}^*, T_{n_p}, \rho_{n_p}}^{\text{exp}} \frac{\partial \delta_{n_p}}{\partial \rho_c} \\ p_{n_p} & \dots & p_{n_p} & p_{n_p} & p_{n_p} \end{array} \right] \quad (29)$$

$$J_{\text{tot}}([\theta_{\text{EOS}}^*, T_c, \rho_c], T, \rho, p) = \left[\begin{array}{c} J_p([\theta_{\text{EOS}}^*, T_c, \rho_c], T, \rho) \\ J_{p_v}([\theta_{\text{EOS}}^*, T_c, \rho_c], T, p) \\ J_{c_v}([\theta_{\text{EOS}}^*, T_c, \rho_c], T, \rho) \\ J_{c_p}([\theta_{\text{EOS}}^*, T_c, \rho_c], T, \rho) \\ J_w([\theta_{\text{EOS}}^*, T_c, \rho_c], T, \rho) \\ J_B([\theta_{\text{EOS}}^*, T_c, \rho_c], T) \\ J_{c_{p0}}([\theta_{\text{EOS}}^*, T_c, \rho_c], T) \\ J_{T_c} \\ J_{\rho_c} \end{array} \right] \quad (32)$$

699 where tot means total. 706
700 The Jacobian $J_{\text{tot}}([\theta_{\text{EOS}}^*, T_c, \rho_c], T, \rho, p)$ is a 707
701 $(n_p + 2n_{p_v} + n_{c_v} + n_{c_p} + n_w + n_B + n_{c_{p0}} + n_{T_c} + n_{\rho_c})$ 708
702 $\times (m + 2)$ matrix. J_{p_v} are functions of T and p 709
703 because their SSE in Eq. (23) have no density 710
704 values as inputs. J_B and $J_{c_{p0}}$ are not functions 711
705 of δ because B and c_{p0} depend on temperature 712

only.

In Eq. (32), with the exception of J_{p_v} , all output variables are assumed to be associated with measurements of temperature and density. However, in actual experiments, other sets of variables like temperature and pressure are more natural independent variables. Hence,

713 conversion for the measurement data point is 737
714 needed before it can be used to calculate the 738
715 Jacobian. For data with temperature and pres- 739
716 sure measurement but unknown density val- 740
717 ues, the density values are calculated from the 741
718 temperature and pressure measurement via the 742
719 EOS. The conversion method for density of dif- 743
720 ferent variables is outlined in Table 2. 744

Table 2: Methods of data conversion for density values in Jacobian calculation

Type of mea- surement	Density values
c_{p0}	Not needed
p, ρ, T	From ρ measurement only
B	Not needed
w, c_p and c_v	Calculated by T and p from EOS

721 According to Eq. (9), the covariance matrix 749
722 can be given as in Eq. (33). 750

723 The size of $COV([\theta_{\text{EOS}}^*, T_c, \rho_c])$ depends on 751
724 the number of parameters in the EOS. For ex- 752
725 ample, the EOS of propane has 97 parameters 753
726 that are obtained from measured data in the 754
727 literature. Taking into account T_c and ρ_c , its 755
728 covariance matrix is a 99×99 square matrix.¹²
729 The EOS of refrigerant R-22 has 55 parameters
730 and its covariance matrix is a 57×57 square ma-
731 trix.⁹

732 Following Eq. (9), the variance σ_p^2 is only mul-
733 tiplied with the elements of $J_p(\theta_{\text{EOS}}^*, \tau, \delta)$; the
734 same holds for the other properties. In order to 756
735 illustrate this, it is possible to re-write Eq. (32) 757
736 in the following way 758

$$V^{-1} \cdot J_{\text{tot}}([\theta_{\text{EOS}}^*, T_c, \rho_c], T, \rho, p) = \begin{bmatrix} 1/\sigma_p^2 \cdot J_p \\ 1/\sigma_g^2 \cdot J_{p_v} \\ 1/\sigma_{c_v} \cdot J_{c_v} \\ 1/\sigma_{c_p}^2 \cdot J_{c_p} \\ 1/\sigma_w^2 \cdot J_w \\ 1/\sigma_B^2 \cdot J_B \\ 1/\sigma_{c_{p0}}^2 \cdot J_{c_{p0}} \\ 1/\sigma_{T_c}^2 \cdot J_{T_c} \\ 1/\sigma_{\rho_c}^2 \cdot J_{\rho_c} \end{bmatrix} \quad (34)$$

The variances σ are essentially weighting factors for the elements of the Jacobian.

To avoid refitting the EOS for the covariance between the coefficients and the critical values, it is assumed that the uncertainties of critical properties have a negligible effect on the estimation of the coefficients θ_{EOS} . The covariance can be written as

$$COV([\theta_{\text{EOS}}^*, T_c, \rho_c]) = \begin{bmatrix} COV(\theta_{\text{EOS}}^*) & 0 & 0 \\ 0 & \frac{\sigma_{T_c}^2}{T_c^2} & 0 \\ 0 & 0 & \frac{\sigma_{\rho_c}^2}{\rho_c^2} \end{bmatrix} \quad (35)$$

745 where $COV(\theta_{\text{EOS}}^*)$ is the submatrix of
746 $COV([\theta_{\text{EOS}}^*, T_c, \rho_c])$ describing the covariances
747 of the EOS parameters but not T_c and ρ_c .
748 $COV(\theta_{\text{EOS}}^*)$ can also be obtained directly by
using Eqs. (32) and (33) when T_c and ρ_c are assumed to be known perfectly and have therefore no uncertainty.

Calculating $COV(\theta_{\text{EOS}}^*)$ based on Eq. (35), it is possible to calculate the respective 95% confidence interval of the EOS parameter values θ_{EOS}

$$\theta_{\text{EOS}, 1-\gamma_t/2} = \theta_{\text{EOS}}^* \pm \sqrt{\text{diag}(COV(\theta_{\text{EOS}}^*))} \cdot t(n-m, \gamma_t/2) \quad (36)$$

In Eq. (36) $t(n-m, \gamma_t/2)$ is the Student t -distribution value corresponding to the $\gamma_t/2$ percentile of the Student t -distribution.

The covariance of the prediction of a certain property is obtained from the respective Jacobian and the parameter covariance matrix and is dimensionalized so that its unit should be the square of that of the property. For example, the covariance $COV(p)$ for a pressure p is given by Eqs. (37) and (38).

where j is a Jacobian vector

The $COV([\theta_{\text{EOS}}^*, T_c, \rho_c])$ is a matrix with elements independent of the input variables to EOS. However, the adjusted Jacobian $j_p([\theta_{\text{EOS}}^*, T_c, \rho_c], T, \rho)$ depends on the value of

$$COV([\theta_{EOS}^*, T_c, \rho_c]) = [J_{tot}([\theta_{EOS}^*, T_c, \rho_c], T, \rho)^T \cdot V^{-1} \cdot J_{tot}([\theta_{EOS}^*, T_c, \rho_c], T, \rho)]^{-1} \quad (33)$$

$$\begin{aligned} COV(p) &= J_p([\theta_{EOS}^*, T_c, \rho_c], T, \rho) \cdot COV([\theta_{EOS}^*, T_c, \rho_c]) \cdot J_p([\theta_{EOS}^*, T_c, \rho_c], T, \rho)^T \cdot p^2 \\ &= j_p([\theta_{EOS}^*, T_c, \rho_c], T, \rho) \cdot COV([\theta_{EOS}^*, T_c, \rho_c]) \cdot j_p([\theta_{EOS}^*, T_c, \rho_c], T, \rho)^T \end{aligned} \quad (37)$$

$$j_p([\theta_{EOS}^*, T_c, \rho_c], T, \rho) = \left[\frac{\partial p}{\partial \theta_1}(\theta_{EOS}^*, T, \rho) \quad \dots \quad \frac{\partial p}{\partial \theta_M}(\theta_{EOS}^*, T, \rho) \quad \frac{\partial p}{\partial T_c}(\theta_{EOS}^*, T, \rho) \quad \frac{\partial p}{\partial \rho_c}(\theta_{EOS}^*, T, \rho) \right] \quad (38)$$

771 T or ρ for the prediction. In complete analogy 805
 772 the covariance matrix is obtained for purely pre- 806
 773 dicted properties such as entropy s by Eqs. (39) 807
 774 and (40). The covariance matrix of other pre-
 775 dicted properties (e.g. u , h , a , g , ϕ and C) can
 776 be calculated in a similar manner.

777 The calculation of the two covariance matrices
 778 is numerically not trivial. The parameter
 779 covariance matrix $COV([\theta_{EOS}^*, T_c, \rho_c])$ is the-
 780oretically obtained through an inversion (see
 781 Eq. (33)). However, both the Jacobians and the
 782 parameter covariance matrices are very large 808
 783 sparse matrices and the parameter covariance 809
 784 matrix can also be positive semi-definite, which 810
 785 means it has columns that are numerically close 811
 786 to being linearly dependent. We recommend 812
 787 the following procedure to overcome these is- 813
 788sues: 814

- 789 1. In order to store more significant digits of 816
 790 matrix elements and to allow more precise 817
 791 matrix operations compared to ordinary 818
 792 algebraic calculation of matrices, we recom- 819
 793 mend the usage of arbitrary precision 820
 794 methods, such as *mpmath* in the Python 821
 795 programming language. 822
- 796 2. For the calculation of the covariance matrices 823
 797 of the properties, e.g. $COV(p)$ or 824
 798 $COV(s)$, we have used LU decomposi- 825
 799 tion. The calculation is shown in the sup- 826
 800 porting information. 827
 828

801 Having obtained the respective covariance 829
 802 matrices of the properties, it is now possible 830
 803 to calculate the 95% confidence interval of the 831
 804 respective properties. Eqs. (41) and (42) allow 832

for a calculation of the 95% confidence interval
 for pressure p and entropy s . The same holds
 for the other properties.

$$p_{1-\gamma_t/2}^{\text{pred}} = p^{\text{pred}} \pm \sqrt{\text{diag}(COV(p))} \cdot t(n-m, \gamma_t/2) \quad (41)$$

$$s_{1-\gamma_t/2}^{\text{pred}} = s^{\text{pred}} \pm \sqrt{\text{diag}(COV(s))} \cdot t(n-m, \gamma_t/2) \quad (42)$$

It is important to notice that in this study
 the sum of squared errors and the Jacobian of
 the fitted properties used relative values, i.e.
 the residuals and the derivatives have been di-
 vided by the corresponding experimental value.
 This corresponded to the objective function for
 the fitting of the parameters used by Lem-
 mon *et al.*¹² However, this means that the co-
 variance matrices provide the relative uncer-
 tainties, which subsequently need to be mul-
 tiplied with the corresponding predicted ther-
 modynamic property from the EOS, in order to
 obtain the absolute uncertainty range as shown
 in Eqs. (41) and (42).

Similar methods can be used to calculate the
 uncertainties of the differences of properties be-
 cause covariance of differences or sums of prop-
 erties can be calculated in a similar manner.
 This is especially important for properties like
 u , s , h , a and g , in which only the differ-
 ence of values matters in EOS applications.
 For example, to calculate the uncertainty of
 the difference of two entropy values $s_1(T_1, \rho_1)$
 and $s_2(T_2, \rho_2)$, one can first calculate the Jaco-
 bian of the difference between the two values

$$COV(s) = j_s([\theta_{\text{EOS}}^*, T_c, \rho_c], T, \rho) \cdot COV([\theta_{\text{EOS}}^*, T_c, \rho_c]) \cdot j_s([\theta_{\text{EOS}}^*, T_c, \rho_c], T, \rho)^T \quad (39)$$

$$j_s([\theta_{\text{EOS}}^*, T_c, \rho_c], T, \rho) = \left[\frac{\partial s}{\partial \theta_1}(\theta_{\text{EOS}}^*, T, \rho) \quad \dots \quad \frac{\partial s}{\partial \theta_M}(\theta_{\text{EOS}}^*, T, \rho) \quad \frac{\partial s}{\partial T_c}(\theta_{\text{EOS}}^*, T, \rho) \quad \frac{\partial s}{\partial \rho_c}(\theta_{\text{EOS}}^*, T, \rho) \right] \quad (40)$$

833 by Eq. (43) and calculate the covariance using
834 Eq. (44).

$$j_{s_1-s_2}([\theta_{\text{EOS}}^*, T_c, \rho_c], T, \rho)^T = \begin{bmatrix} \frac{\partial s_1}{\partial \theta_1}(\theta_{\text{EOS}}^*, T_1, \rho_1) - \frac{\partial s_2}{\partial \theta_1}(\theta_{\text{EOS}}^*, T_2, \rho_2) \\ \vdots \\ \frac{\partial s_1}{\partial \theta_m}(\theta_{\text{EOS}}^*, T_1, \rho_1) - \frac{\partial s_2}{\partial \theta_m}(\theta_{\text{EOS}}^*, T_2, \rho_2) \\ \frac{\partial s_1}{\partial T_c}(\theta_{\text{EOS}}^*, T_1, \rho_1) - \frac{\partial s_2}{\partial T_c}(\theta_{\text{EOS}}^*, T_2, \rho_2) \\ \frac{\partial s_1}{\partial \rho_c}(\theta_{\text{EOS}}^*, T_1, \rho_1) - \frac{\partial s_2}{\partial \rho_c}(\theta_{\text{EOS}}^*, T_2, \rho_2) \end{bmatrix} \quad (43)$$

835 The uncertainty of the difference between s_1 840
836 and s_2 can be calculated by Eq. (45).

837 3.2 Properties with inputs other 838 than T and ρ

In practical applications of EOS, there are many scenarios where the inputs to the EOS are not temperature and density. For example, a user may be given the measured temperature and pressure of a fluid to find the speed of sound, and the user must use an iterative solver to find the density of the fluid first before calculating the speed of sound. For substances that are either superheated vapor or subcooled liquid, if the output variable required is neither temperature nor density, the calculation of the uncertainty of the output variable will follow that in Section 3.1 after calculating the missing temperature and density values by using an iterative solver on the EOS. However, if the output variable is either temperature or density, the uncertainty of the output variable should be calculated by propagating the uncertainty of the input variable due to the EOS to the output using the linearization of the EOS.^{23,33} This is

done by Eqs. (46) and (47).

$$\Delta T^{\text{pred}} = \left| \left(\frac{\partial T^{\text{pred}}}{\partial x_1} \Big|_{x_2} \Delta x_1 \right) + \left(\frac{\partial T^{\text{pred}}}{\partial x_2} \Big|_{x_1} \Delta x_2 \right) \right| \quad (46)$$

$$\Delta \rho^{\text{pred}} = \left| \left(\frac{\partial \rho^{\text{pred}}}{\partial x_1} \Big|_{x_2} \Delta x_1 \right) + \left(\frac{\partial \rho^{\text{pred}}}{\partial x_2} \Big|_{x_1} \Delta x_2 \right) \right| \quad (47)$$

839 where Δx is the standard uncertainty of variable x , T^{pred} and ρ^{pred} are the temperature and density values predicted by using an iterative solver with the EOS, x_1 and x_2 are the independent variables used to predict T^{pred} or ρ^{pred} , Δx_1 and Δx_2 are the EOS uncertainties of the variables x_1 and x_2 calculated by using the temperature and density values in Eq. (42), and the partial derivatives are obtained according to Thorade and Saadat.³⁴

If any of x_1 and x_2 in Eqs. (46) and (47) are T or ρ , their corresponding uncertainties in these equations will be zero.

Since the use of Eqs. (46) and (47) is a result of the difficulty to define covariance of temperature and density, calculating the uncertainties of the sums and differences of temperature and density with equations similar to Eq. (45) is impossible. Hence the calculation of the uncertainties of the sums and differences of temperature and density is the same as that of ordinary variables and follows the method in Kline and McClintock.²³

862 3.3 Saturated liquid and vapor 863 properties

864 Calculation of thermodynamic properties of a
865 fluid that is based on temperature and density

$$COV(s_1 - s_2) = j_{s_1-s_2}([\theta_{EOS}^*, T_c, \rho_c], T, \rho) \cdot COV([\theta_{EOS}^*, T_c, \rho_c]) \cdot j_{s_1-s_2}([\theta_{EOS}^*, T_c, \rho_c], T, \rho)^T \quad (44)$$

$$s_{1,1-\gamma_t/2}^{\text{pred}} - s_{2,1-\gamma_t/2}^{\text{pred}} = s_1 - s_2 \pm \sqrt{\text{diag}(COV(s_1 - s_2))} \cdot t(n - m, \gamma_t/2) \quad (45)$$

values for a homogeneous phase can be achieved by the procedure in Section 3.1. However, users of EOS are often asked for fluid properties of saturated liquid and vapor of a fluid given a temperature or pressure value only. According to Lemmon *et al.*,¹² this is achieved by finding two density values for which Gibbs energy and pressure values are equivalent at the given temperature value – this is the Maxwell’s criteria. The smaller density value corresponds to the density of saturated vapor whereas the larger density value corresponds to the density of saturated liquid, and the other properties of saturated liquid and vapor can be calculated from the density values. The uncertainty of the thermodynamic properties (calculated through the equations in ??) can be calculated in the same manner as that in Section 3.1 once the density values are found. The calculation of the residuals in the Maxwell criteria is given by Eqs. (48) and (49).

$$res_1 = g(\rho_v, T) - g(\rho_l, T) \quad (48)$$

$$res_2 = p(\rho_v, T) - p(\rho_l, T), \quad (49)$$

where *res* is a residual function.

where res_1 and res_2 are residual functions of the Maxwell criteria. By finding the density values that lead to zero values for both residual functions, the saturation densities of the fluid at a certain temperature T can be found.

The uncertainty of the Gibbs energy difference in Eq. (48) given by Δres_1 can be calculated by calculating the covariance of the Gibbs energy values from Eq. (52).

The uncertainties of the density values can then be calculated by propagating the uncertainties of the residual functions as shown in

Eqs. (50) and (51).

$$= \left| \left(\frac{\partial res_1}{\partial \rho_l} \Big|_T \right)^{-1} \Delta res_1 + \left(\frac{\partial res_2}{\partial \rho_l} \Big|_T \right)^{-1} \Delta res_2 \right| \quad (50)$$

$$= \left| \left(\frac{\partial res_1}{\partial \rho_v} \Big|_T \right)^{-1} \Delta res_1 + \left(\frac{\partial res_2}{\partial \rho_v} \Big|_T \right)^{-1} \Delta res_2 \right| \quad (51)$$

However, Δres_2 in Eqs. (50) and (51) involves uncertainty of pressure of saturated liquid that changes very nonlinearly with respect to density. The rapid changes of the sensitivity of saturated liquid pressure with density renders linear error propagation to be invalid to calculate the uncertainties in Eqs. (50) and (51). To calculate Δres_2 for the linear error propagation in Eqs. (50) and (51), the uncertainty of the Gibbs energy difference in Eq. (52) is used to approximate the uncertainty of difference of pressure values as shown in Eq. (53).

$$\Delta res_2 = \frac{p \Delta res_1}{RT} \quad (53)$$

Equation (53) is used because the relative difference of Gibbs energy between saturated liquid and vapor changes proportionally with the difference of estimated and measured saturated pressure as shown in Fig. 1.

Since residual functions calculate the differences of Gibbs energy and pressure respectively, the uncertainties of the corresponding Gibbs energy and pressure at saturation are given by the uncertainties of the residual functions as shown in Eqs. (54) and (55).

$$\Delta res_1 = \sqrt{\text{diag}(\text{COV}(g(\rho_v, T) - g(\rho_l, T)))} \cdot t(n - m, \gamma_t/2) \quad (52)$$

$$\Delta g_{\text{sat}} = \Delta res_1 \quad (54)$$

$$\Delta p_{\text{sat}} = \Delta res_2 \quad (55)$$

where sat means saturation.

With the approximation in Eq. (53), the uncertainties of p and g at saturation in Eqs. (54) and (55) and the definition of fugacity, the uncertainty of fugacity coefficient ϕ at saturation can be derived to be zero and the relative uncertainty of fugacity equals to the relative uncertainty of pressure at saturation in Eq. (55).

However, other thermodynamic properties at the saturated states are calculated by solving the original EOS with the density values from the Maxwell criteria and the original temperature input to the Maxwell criteria. The calculation would propagate the uncertainties calculated from Eqs. (50) and (51), and the uncertainties from Eqs. (50) and (51) will be added to the uncertainties from Eq. (42) to calculate the uncertainties of these thermodynamic properties. For example, the uncertainty of entropy of saturated liquid and saturated vapor are calculated by adding the uncertainties as Eqs. (56) and (57).

$$\Delta s_l = \sqrt{\text{diag}(\text{COV}(s(T, \rho_l))) \cdot t(n - m, \gamma_t/2)^2 + \left(\frac{\partial s_l}{\partial T} \Big|_{\text{sat}} \Delta T + \frac{\partial s_l}{\partial \rho_l} \Big|_{\text{sat}} \Delta \rho_l \right)^2} \quad (56)$$

$$\Delta s_v = \sqrt{\text{diag}(\text{COV}(s(T, \rho_v))) \cdot t(n - m, \gamma_t/2)^2 + \left(\frac{\partial s_v}{\partial T} \Big|_{\text{sat}} \Delta T + \frac{\partial s_v}{\partial \rho_v} \Big|_{\text{sat}} \Delta \rho_v \right)^2} \quad (57)$$

where l means saturated liquid and v is saturated vapor.

When the uncertainty of the differences between the entropy of saturated liquid or vapor and an entropy value in a homogeneous phase

is needed, the calculation can be carried out by Eqs. (58) and (59).

The uncertainty of the entropy of vaporization can be calculated by Eq. (60).

Uncertainties of other properties (e.g., u , h , a , c_p , c_v and ϕ) of saturated liquid and vapor can be calculated in a similar manner as Eqs. (56) and (57). Numerically, the uncertainties can also be calculated from Eq. (42) with density and temperature of the saturated liquid and vapor, but Eq. (42) does not include the uncertainty in the EOS caused by the Maxwell criteria and underestimates the uncertainties. Hence when the uncertainties of properties at saturation are needed, Eqs. (56) and (57) should be used to calculate the uncertainties of entropy of the saturated liquid and vapor instead.

Properties other than temperature can be used as inputs to the EOS to calculate the thermodynamic properties of saturated states; for instance pressure can be used as an input to find the saturation temperature of a fluid at that pressure. To calculate the uncertainty of saturation temperature, the uncertainty of pressure in Eq. (55) can be used to propagate the uncertainty of the EOS to the saturation temperature value, and the uncertainty of saturation temperature can be calculated by Eq. (61).

$$\Delta T_{\text{sat}} = \left| \left(\frac{dT}{dp} \Big|_{\text{sat}} \right) \Delta p_{\text{sat}} \right| \quad (61)$$

where $\frac{dT}{dp} \Big|_{\text{sat}}$ is calculated by the Clapeyron relation as shown in Eq. (62).²⁹

$$\frac{dT}{dp} \Big|_{\text{sat}} = \frac{1/\rho_l - 1/\rho_v}{s_v - s_l} \quad (62)$$

and the uncertainty in vapor pressure Δp_{sat} is obtained from Eq. (53).

$$\Delta(s_l - s_{1p}) = \sqrt{\text{diag}(\text{COV}(s(T, \rho_l) - s_{1p}(T_{1p}, \rho_{1p}))) \cdot t(n - m, \gamma_t/2)^2 + \left(\frac{\partial s_l}{\partial T} \Big|_{\text{sat}} \Delta\rho_l \right)^2} \quad (58)$$

$$\Delta(s_v - s_{1p}) = \sqrt{\text{diag}(\text{COV}(s(T, \rho_v) - s_{1p}(T_{1p}, \rho_{1p}))) \cdot t(n - m, \gamma_t/2)^2 + \left(\frac{\partial s_v}{\partial T} \Big|_{\text{sat}} \Delta\rho_v \right)^2} \quad (59)$$

$$\Delta(s_v - s_l) = \sqrt{\text{diag}(\text{COV}(s(T, \rho_v) - s(T, \rho_l))) \cdot t(n - m, \gamma_t/2)^2 + \left(\frac{\partial s_l}{\partial T} \Big|_{\text{sat}} \Delta\rho_l - \frac{\partial s_v}{\partial T} \Big|_{\text{sat}} \Delta\rho_v \right)^2} \quad (60)$$

3.4 Thermodynamic quality

When defining the thermodynamic state of liquid and vapor phases in equilibrium of a pure substance, an additional property called thermodynamic quality as defined by

$$q = \frac{1/\rho - 1/\rho_l(T)}{1/\rho_v(T) - 1/\rho_l(T)} \quad (63)$$

where q is thermodynamic quality, is commonly used, where ρ_l is the density of saturated liquid, ρ_v is the density of saturated vapor, q is the thermodynamic quality and $\rho_v \leq \rho \leq \rho_l$.

Although q is not given as part of an output of a part of Helmholtz-based EOS, it is commonly computed as an internal function in software packages calculating thermodynamic properties, and hence it is necessary to define its uncertainty calculation. From Eq. (63), it can be seen that the uncertainty of thermodynamic quality due to EOS mainly comes from the calculation of the density of the saturated liquid and vapor. By propagating the uncertainty of the density of saturated liquid and vapor, the uncertainty of thermodynamic quality due to the EOS can be calculated by Eq. (64).

$$\Delta q = \left| \frac{\partial q}{\partial \rho_v} \Delta\rho_v + \frac{\partial q}{\partial \rho_l} \Delta\rho_l \right| \quad (64)$$

$$\frac{\partial q}{\partial \rho_l} = \frac{1 - q}{\rho_l^2 \left(\frac{1}{\rho_v} - \frac{1}{\rho_l} \right)} \quad (65)$$

$$\frac{\partial q}{\partial \rho_v} = \frac{q}{\rho_v^2 \left(\frac{1}{\rho_v} - \frac{1}{\rho_l} \right)} \quad (66)$$

where Δq is the uncertainty of the thermodynamic quality, and $\Delta\rho_v$ and $\Delta\rho_l$ are uncertainties calculated in Section 3.3.

If either temperature or density are not given as inputs to the EOS, they will be first calculated by solving the EOS iteratively. The temperature and density values will be used to calculate uncertainty of the thermodynamic quality according to Eq. (64).

3.5 Other thermodynamic properties of two-phase mixtures

The calculation method of the uncertainty of the property from the EOS for two-phase systems with input variables other than temperature and density is different from that in Sections 3.1 and 3.2, because it involves the calculation of the thermodynamic quality. In this case, the uncertainties calculated in Section 3.3 related to the Maxwell criteria are also involved in the calculation of the uncertainties of proper-

1027 ties using thermodynamic quality as one of the 1058
1028 inputs.

1029 When the thermodynamic quality is 0 (satu-
1030 rated liquid) or 1 (saturated vapor), the uncer-
1031 tainty of the properties can be calculated based
1032 on the equations in Section 3.3, and their uncer-
1033 tainties are given by Eqs. (54), (55) and (61). 1059
1034 However, for all other properties, their uncer-1060
1035 tainties are calculated with a different method. 1061
1036 For example, if the uncertainty of an entropy 1062
1037 value is calculated with an intermediate ther-
1038 modynamic property as one of its inputs, to in-1063
1039 clude the uncertainty propagated from the use
1040 of the Maxwell criteria, its calculation will be 1064
1041 carried out with Eq. (67).

$$\begin{aligned}
 & \Delta s_{2p} \\
 = & \sqrt{\frac{\left(\frac{\partial s_{2p}}{\partial q}\Big|_T \Delta q\right)^2}{+\text{diag}(\text{COV}(s_{2p})) \cdot t(n-m, \gamma_t/2)^2}} \\
 = & \sqrt{\frac{[(s_v - s_l)\Delta q]^2}{+\text{diag}(\text{COV}(s_{2p})) \cdot t(n-m, \gamma_t/2)^2}}
 \end{aligned} \tag{67}$$

1042 where 2p is two-phase.

1043 where the subscript 2p means two-phase fluid.

1044 For the uncertainty of its difference with en-1078
1045 tropy values in single phase, the uncertainty can 1079
1046 be calculated by Eq. (68).

$$\begin{aligned}
 & \Delta(s_{2p}(T_{2p}, q_{2p}) - s_{1p}) \\
 = & \sqrt{\frac{[(s_v(T_{2p}) - s_l(T_{2p}))\Delta q_{2p}]^2}{+\text{diag}(\text{COV}(s_{2p} - s_{1p})) \cdot t(n-m, \gamma_t/2)^2}}
 \end{aligned} \tag{68}$$

1047 where 1p is one-phase.

1048 When the uncertainty of its difference with 1088
1049 entropy values of the saturated liquid or vapor 1089
1050 is needed, the uncertainty can be calculated by 1090
1051 Eqs. (69) and (70). 1091

1052 The uncertainty of the difference between a 1092
1053 pair of two-phase entropy states can be calcu-1093
1054 lated by Eq. (71). The uncertainty of properties 1094
1055 u , h and a can also be calculated in a manner 1095
1056 similar to Eqs. (67) to (70). 1096

1057 The uncertainty of density can be calculated 1097

from

$$\Delta \rho_{2p} = \sqrt{\left(\frac{-1/\rho^2}{1/\rho_v - 1/\rho_l} \Delta q\right)^2 + (\Delta \rho)^2}, \tag{72}$$

where $\Delta \rho$ comes from Eq. (47).

The properties c_p and w are undefined for two-phase states and therefore do not have any uncertainty values associated with them.

3.6 Summary

Figure 2 summarizes the choice of uncertainty calculation method of the EOS based on the input variables and the phase of the fluid where the uncertainty of a property value is needed.

When the input variables are temperature and density, the calculation method follows the basic uncertainty calculation method derived in Section 3.1 because the calculation does not involve the determination of the phase of the fluid nor any iterative calculation. If the input variables are not temperature and density, the EOS would involve iterative calculation. For superheated vapor and subcooled liquid, the method should follow Section 3.2. For saturated vapor and liquid, the calculation involves the Maxwell criteria and Section 3.3 should be followed. For two-phase states, if the output is Gibbs energy, pressure, fugacity coefficient or temperature, the calculation method would be the same as that of saturated liquid and vapor, and the method in Section 3.3 should be followed. If the output is thermodynamic quality, the uncertainty calculation method in Section 3.4 should be used. Otherwise, the uncertainty calculation method in Section 3.5 should be followed.

When the differences of properties are needed, the calculation steps of the uncertainties follow the flowchart in Fig. 3

If the difference involves T , ρ , or q , whose covariance cannot be calculated directly, the uncertainty of the differences will be calculated by propagating the uncertainties of individual property values with methods in Kline and McClintock.²³ If the inputs are all T and ρ , no Maxwell criteria will be involved even for two-

$$\Delta(s_{2p}(T_{2p}, q_{2p}) - s_1(T_1)) = \sqrt{\text{diag}(COV(s_{2p}(T_{2p}, q_{2p}) - s_1(T_1))) \cdot t(n - m, \gamma_t/2)^2 + \left(\frac{\partial s_1(T_1)}{\partial T} \Big|_{\text{sat}} \Delta\rho_1(T_1) - [(s_v(T_{2p}) - s_1(T_{2p}))\Delta q_{2p}] \right)^2} \quad (69)$$

$$\Delta(s_{2p}(T_{2p}, q_{2p}) - s_v(T_v)) = \sqrt{\text{diag}(COV(s_{2p}(T_{2p}, q_{2p}) - s_v(T_v))) \cdot t(n - m, \gamma_t/2)^2 + \left(\frac{\partial s_v(T_v)}{\partial T} \Big|_{\text{sat}} \Delta\rho_v(T_v) - [(s_v(T_{2p}) - s_1(T_{2p}))\Delta q_{2p}] \right)^2} \quad (70)$$

1100 phase substances, and the uncertainty of prop-1121
 1101 erty differences can be calculated directly fol-1122
 1102 lowing Section 3.1. If the difference involves 1123
 1103 two-phase states, the property calculation fol-1124
 1104 lows that listed in Section 3.5. If the difference 1125
 1105 involves saturated liquid or vapor, the method 1126
 1106 to calculate the uncertainty of property differ-1127
 1107 ences in Section 3.3. Otherwise, the calculation 1128
 1108 method of uncertainty methods listed in Sec-1129
 1109 tion 3.1 will be used.

1110 The Python code used to calculate the uncer-1130
 1111 tainties is listed in the Supplementary Materials 1131
 1112 for reference. 1132

1113 4 Results and Discussion 1135

1114 To illustrate the application of the proposed un-1137
 1115 certainty calculation method, it is applied to 1138
 1116 the EOS of propane.¹² Its EOS is Helmholtz-1139
 1117 energy-explicit, and the proposed uncertainty 1140
 1118 calculation method can be applied to it to 1141
 1119 demonstrate how uncertainties of the EOS af-1142
 1120 fect the properties estimated by the EOS. 1143

4.1 Experimental data

The experimental data used in this work were obtained via NIST ThermoDataEngine (TDE) #103b.^{35–38} The data sources are summarized in Table 3, and a more detailed list of the experimental data considered is provided in the Supporting Data. These data span several different types, including densities, saturation properties (vapor pressure, latent heat of vaporization, etc.) and properties in homogeneous phases (speed of sound, heat capacities, etc.).

The resultant normalized σ values in Eq. (26) that are calculated based on the deviations between the data in Table 3 and the estimation from the EOS are listed in Table 4. These σ values come from the relative deviations between the EOS and the measurement results. The relative deviation between measurement data and the EOS estimation of pressure from the data sets of liquid and vapor density yield the largest values in Table 4. It can be seen that the major source of uncertainties come from the deviations of the measurement data of density of liquid and vapor with the EOS estimation. The relative deviations between measurement and

$$\Delta(s_{2p,1}(T_{2p,1}, q_{2p,1}) - s_{2p,2}(T_{2p,2}, q_{2p,2})) = \sqrt{\text{diag}(COV(s_{2p,1} - s_{2p,2})) \cdot t(n - m, \gamma_t/2)^2 + \left([(s_v(T_{2p,1}) - s_1(T_{2p,1}))\Delta q_{2p,1}] - [(s_v(T_{2p,2}) - s_1(T_{2p,2}))\Delta q_{2p,2}] \right)^2} \quad (71)$$

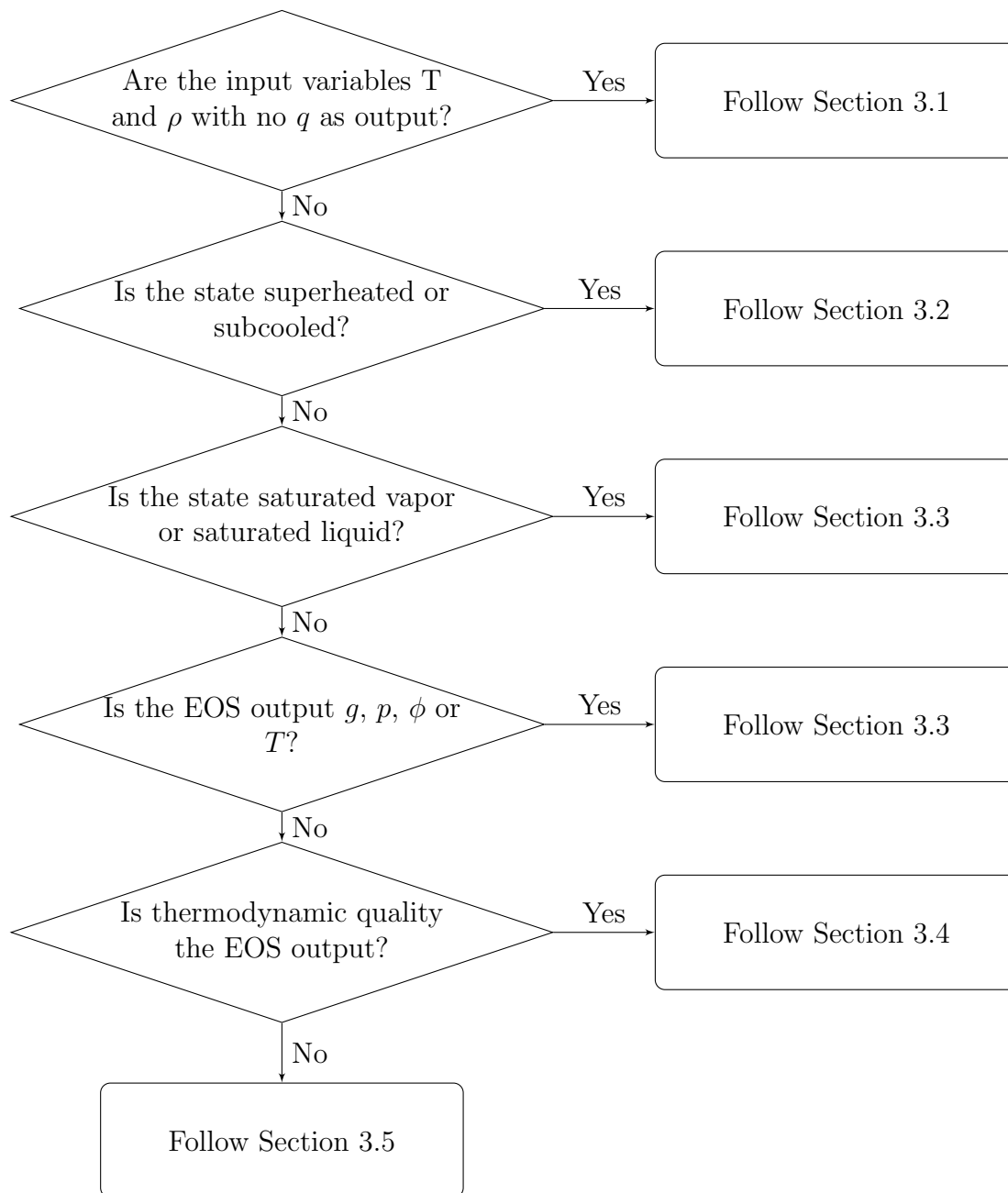


Figure 2: Flowchart showing the choice of equations to calculate the uncertainties of EOS based on the input variables and state of the fluid

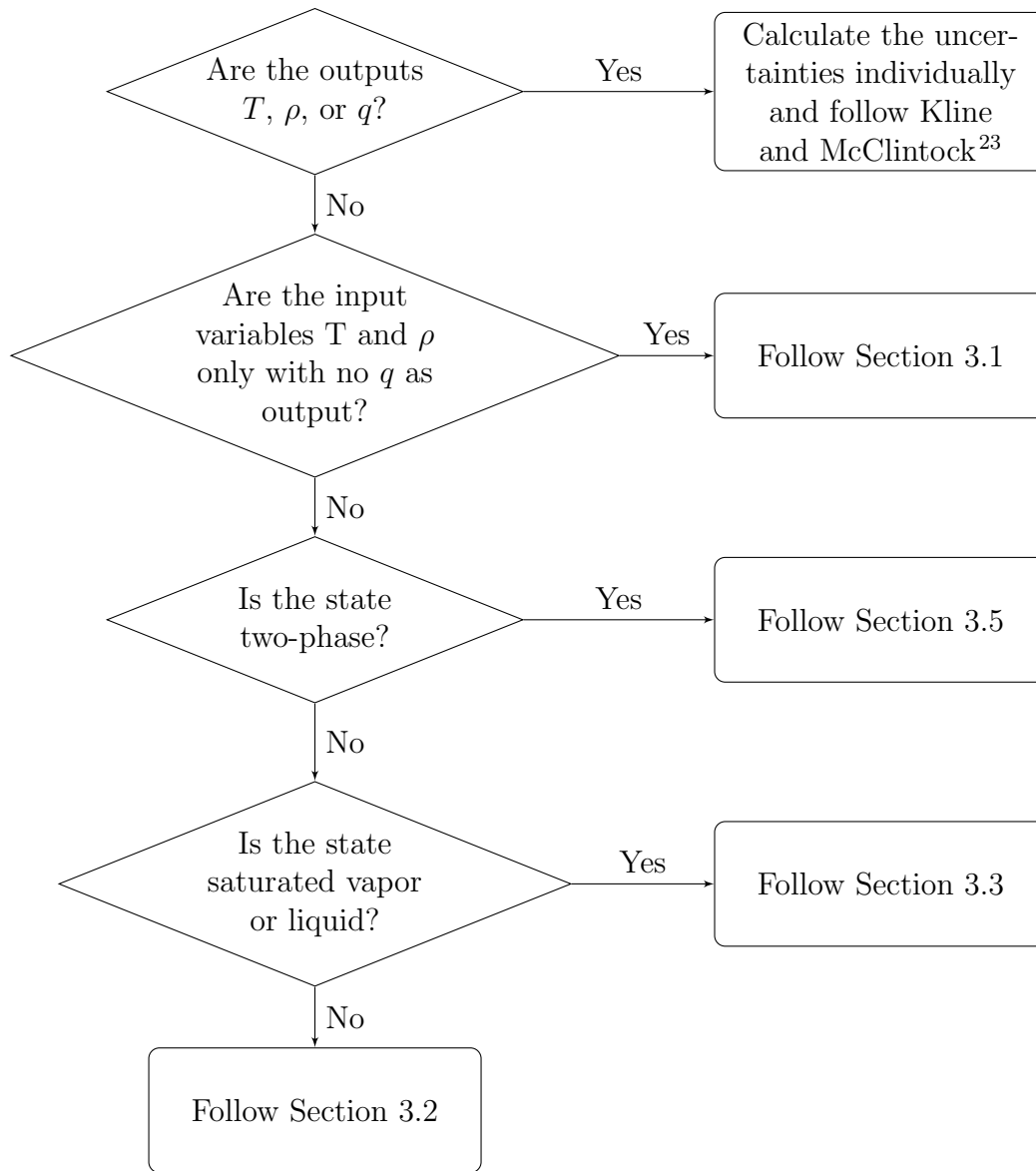


Figure 3: Flowchart showing the choice of equations to calculate the uncertainties of property differences

1146 the EOS estimation of specific heat capacity₁₁₆₀
 1147 of liquid and vapor, saturation pressure, σ ₁₁₆₁
 1148 and virial coefficient and speed of sound also₁₁₆₂
 1149 contribute to the uncertainties of the EOS sig₁₁₆₃
 1150 nificantly. However, the relative deviations be₁₁₆₄
 1151 tween measurement and the EOS estimation of₁₁₆₅
 1152 ideal gas specific heat capacity, critical temper₁₁₆₆
 1153 ature and critical density are much smaller than₁₁₆₇
 1154 that of the other properties, and they do not₁₁₆₈
 1155 contribute to the uncertainty of the EOS as₁₁₆₉
 1156 significantly as the measurement of the other₁₁₇₀
 1157 properties. 1171

1158 Table 4 also shows the corresponding stan₁₁₇₂
 1159 dard measurement uncertainty of different₁₁₇₃

property values that are converted. These
 uncertainty values were taken from Thermo-
 DataEngine and represent a combination of
 experimental uncertainties ascribed by the indi-
 vidual researcher as well as, when appropriate,
 expert evaluation to increase the uncertainty
 to a more reasonable value if the claimed un-
 certainty is not reasonable. These standard
 uncertainty values are calculated by averag-
 ing the standard measurement uncertainties of
 the measurement data, and they can be com-
 pared directly with the normalized σ values.
 The results show that the noramlized σ are not
 significantly larger than their corresponding

Table 3: Summary of experimental data from TDE considered in this study. Any experimental data points flagged by TDE as being unreliable were not included.

Data type	N	T range K	p range MPa
T_c	45		
p_c	38		
ρ_c	18		
p_{sat}	1392	85 to 369	1.6332×10^{-10} to 4.91426
Liquid ρ	3746	88 to 369	0.3546 to 1072.7
Saturated Liquid ρ	528	86 to 369	
Vapor ρ	3494	243 to 609	0.040934 to 1047
Saturated Vapor ρ	100	230 to 369	
Second Virial Coefficient B	167	183 to 559	
Enthalpy of Vaporization	50	186 to 362	
Liquid c_p	108	89 to 366	0.101325 to 5.43
Vapor c_p	138	273 to 573	0.049033 to 10.3421
c_{p0}	50	148 to 353	
Homogeneous Phase c_p	110	100 to 374	
Liquid w	655	90 to 339	1.92 to 60.58
Saturated Vapor w	59	90 to 325	
Vapor w	423	225 to 375	0.01008 to 0.8513
Homogenous Phase w	593	239 to 498	9.80665×10^{-6} to 101.337

1174 measurement uncertainties with the exception¹¹⁹⁶
1175 of the second virial coefficient and the speed of¹¹⁹⁷
1176 sound. For these two variables, the normalized¹¹⁹⁸
1177 σ are at least 100.0% larger than their mea-¹¹⁹⁹
1178 surement counterparts. The normalized σ for¹²⁰⁰
1179 p from data sets of liquid and vapor ρ is also¹²⁰¹
1180 much larger than the relative standard mea-¹²⁰²
1181 surement uncertainty of p values at saturation.¹²⁰³
1182 The results show that the inaccuracy of EOS¹²⁰⁴
1183 estimation may also play a critical role in the¹²⁰⁵
1184 uncertainty of EOS besides the measurement¹²⁰⁶
1185 uncertainty of the experimental data.

1186 We present the results in three parts. First¹²⁰⁷
1187 the parameter identifiability is analyzed. Then¹²⁰⁸
1188 the uncertainties of saturation properties are¹²⁰⁹
1189 studied. Finally the variation of uncertainties¹²¹⁰
1190 with the thermodynamic state points are pre-¹²¹¹
1191 sented and discussed.¹²¹²

1192 4.2 Covariance, correlation ma- 1193 trix and identifiability¹²¹⁴

1194 Considering the parameter covariance matrix¹²¹⁷
1195 (as calculated by Eq. 9) it is also possible¹²¹⁸

to assess the parameter identifiability. The
square-root of the diagonal elements of the
covariance matrix (i.e. $\sqrt{\text{diag}(\text{COV}(\theta_{\text{EOS}}^*))}$)
correspond to the parameter standard devia-
tion. If the standard deviations with respect to
the parameter values are large, parameters are
not practically identifiable. This means that
there are not enough data to estimate the pa-
rameters with the current model and objective
function. We chose as a metric for practical
identifiability: $\left| \frac{\sqrt{\text{diag}(\text{COV}(\theta_{\text{EOS}}^*))}}{\theta_{\text{EOS}}^*} \right|$. In
the given study nearly all the parameters (be-
sides n_{16} and n_{17}) have a small standard de-
viation compared to the parameter value, i.e.
 $\left| \frac{\sqrt{\text{diag}(\text{COV}(\theta_{\text{EOS}}^*))}}{\theta_{\text{EOS}}^*} \right| < 0.1$ (see the Sup-
porting Information). This result implies that
the amount of experimental data used for the
parameter fitting (see Lemmon *et al.*¹²) and
the uncertainty analysis is sufficiently high to
guarantee the identification of the parameters
from the data. A small amount of experimen-
tal data would lead to poor identifiability and
therefore parameter values with large standard

Table 4: Normalized σ values from deviations between measurement and EOS estimation in Eq. (26) for propane, and their corresponding average relative standard measurement uncertainty

Property	Normalized σ	Corresponding average relative standard uncertainty
c_{p0}	5.104×10^{-3}	1.448 %
c_p	8.113×10^{-2}	4.391 %
c_v	7.021×10^{-2}	1.081 %
Saturated liquid and vapor p	2.661×10^{-2}	5.228 %
p from data sets of liquid and vapor ρ	1.465×10^{-1}	Not available
ρ_c	4.447×10^{-6}	1.306 %
T_c	7.767×10^{-6}	0.100 %
B	3.880×10^{-2}	1.623 %
w	6.388×10^{-2}	0.196 %

1219 deviations. It is recommended that develop-1248
1220 ers of Helmholtz-type EoS analyze the parame-1249
1221 ter covariance matrix with respect to parameter1250
1222 identifiability in order to ensure that sufficient1251
1223 experimental data has been used for the fitting1252
1224 of the respective parameters. 1253

1225 The parameter correlation matrix (obtained1254
1226 by Eq. 10), contains information of the corre-1255
1227 lation coefficients between the parameters; the1256
1228 parameter correlation matrix is attached in the1257
1229 supplementary material. Several of the parame-1258
1230 ters are highly correlated, corresponding to high1259
1231 correlation coefficients $> \pm 0.7$ (a correlation co-1260
1232 efficient equal to 1 would correspond to a per-1261
1233 fect correlation). This means that many param-1262
1234 eters are not independent from each other, due1263
1235 to the structure of the equations: Parameters1264
1236 increase or decrease, when other ones increase1265
1237 or decrease. However, due to the fact that a suf-1266
1238 ficiently large amount of experimental data has1267
1239 been used for the calculation, the high correla-1268
1240 tion coefficients did not lead to high parameter1269
1241 uncertainties. 1270

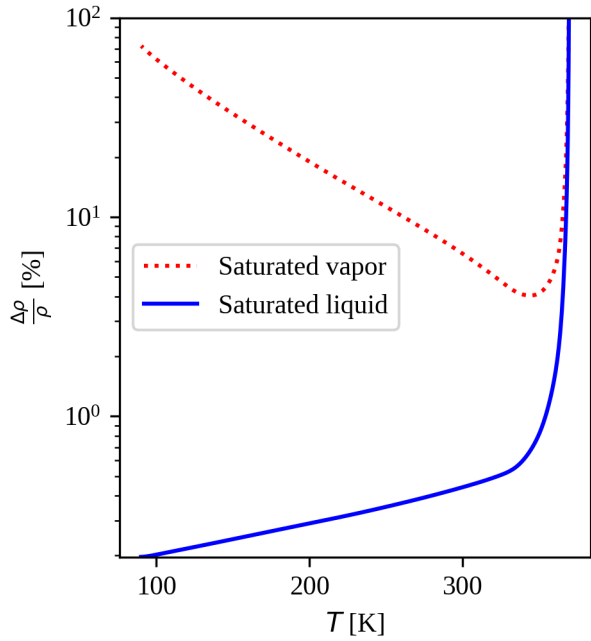
1242 4.3 Saturated property uncer-1272 1243 tainty 1273 1274

1244 To understand the magnitude of uncertain-1275
1245 ties of various properties within the applica-
1246 ble range of the EOS, the uncertainties of den-1276
1247 sity and enthalpy along the saturation curves1277

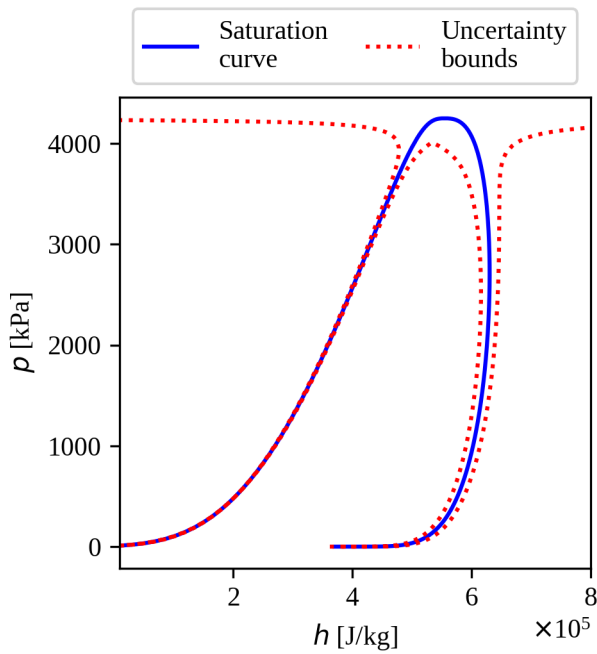
are plotted from the triple point temperature
of 85.525 K to the critical temperature¹² with
uncertainty bounds overlaid as shown in Fig. 4.

The uncertainties in Figure 4 are reasonable
at most conditions except near the critical point
in both diagrams and at low temperature for
saturated vapor in Fig. 4a. The uncertainties
of properties near the critical point are much
larger than ones further from the critical point,
which is also reported in Lemmon *et al.*¹² with-
out quantification. The reason for the large un-
certainties is due to the mathematical structure
of the Maxwell criteria as shown in Section 3.3.
According to the Maxwell criteria and Eqs. (50)
and (51), the uncertainties of the density of sat-
urated liquid and vapor and hence the uncer-
tainties of other saturated properties depend on
the derivative of densities with respect to pres-
sure and Gibbs energy. As the temperature of
a saturated substance approaches the critical
point, the saturation densities change rapidly
along the saturation line, and the derivatives of
densities with respect to pressure become very
large in magnitude, as shown in Fig. 5.

The trend of the derivative increasing to in-
finity at the critical temperature as shown in
Fig. 5 are unavoidable because critical points
are classically defined as the point where $\left. \frac{\partial \rho}{\partial p} \right|_T$
and $\left. \frac{\partial^2 \rho}{\partial p^2} \right|_T$ are infinite.²⁹ The uncertainties of
saturated liquid and vapor properties depend



(a) Change of relative uncertainty of ρ of saturated liquid and vapor with temperature along the saturation line



(b) p - h diagram with uncertainties of h relative to its reference state

Figure 4: Uncertainties along saturation lines in different property diagrams from 85.525 K to the critical temperature

1278 on the uncertainties of their densities; hence
 1279 their large derivatives with respect to pressure
 1280 near the critical point results in large uncertain-
 1281 ties as shown in Fig. 4.

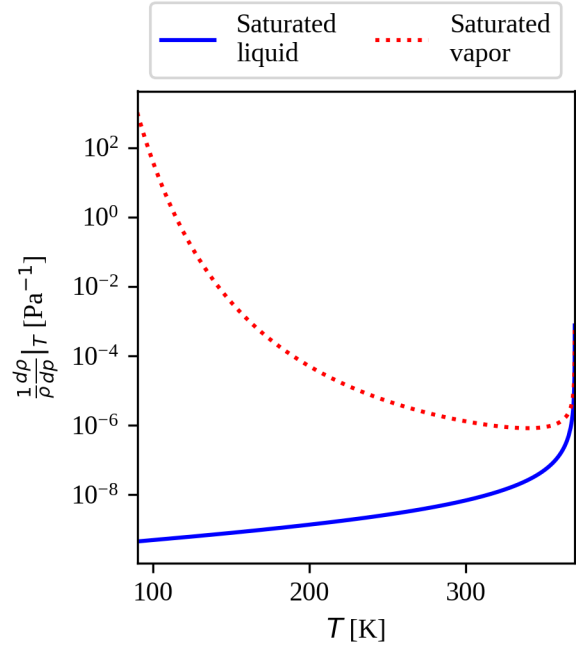
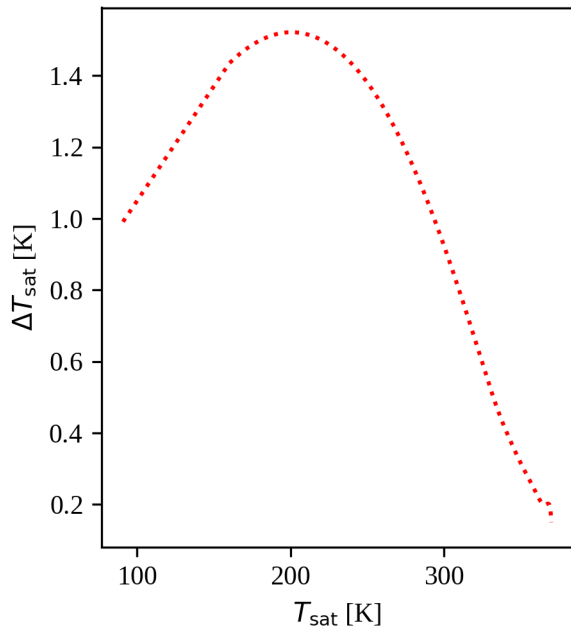


Figure 5: Changes of relative derivatives of density with respect to pressure with temperature from 85.525 K to the critical temperature of propane

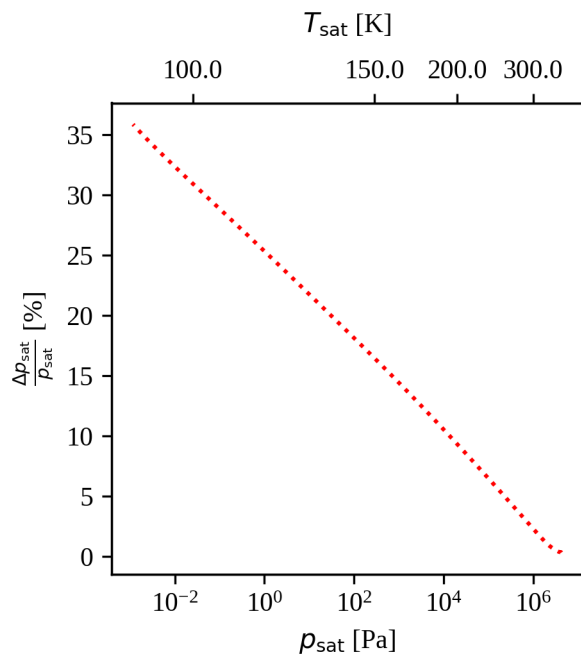
1282 Fig. 5 also explains why the uncertainty of
 1283 saturated vapor is large at low temperature in
 1284 Fig. 4a. The relative derivatives of density of
 1285 saturated vapor with respect to pressure is in-
 1286 creasing with decreasing temperature. These
 1287 increasing derivatives propagate into the uncer-
 1288 tainty of saturated density by Maxwell crite-
 1289 ria, and the uncertainty of density of saturated
 1290 vapor becomes large. In contrast, the relative
 1291 derivative of density of saturated liquid is de-
 1292 creasing with decreasing temperature, and by
 1293 the same uncertainty propagation mechanism,
 1294 the uncertainty of density of saturated liquid
 1295 becomes small at low temperature in Fig. 4a.

1296 To examine the uncertainty of saturation
 1297 pressure along the saturation line, the un-
 1298 certainty of saturation temperature and the
 1299 relative uncertainty of pressure calculated by
 1300 Eq. (73) are plotted with the saturation prop-
 1301 erties in Fig. 6.

$$\text{Relative uncertainty of variable } x = \frac{\Delta x}{x} \quad (73)$$



(a) Changes of uncertainty of saturation temperature with temperature



(b) Changes of relative uncertainty of saturation pressure with pressure

Figure 6: Changes of saturation property uncertainties with their corresponding properties

1303 Figure 6a shows that the uncertainty of sat-
 1304 uration temperature becomes more significant
 1305 at lower temperature. At temperature around
 1306 200 K, the uncertainty peaks at around 1.5 K,
 1307 and it approaches 1 K as the temperature is

1308 lowered to the triple point of propane. How-
 1309 ever, when the uncertainty is studied from the
 1310 perspective of pressure in Figure 6b, the relative
 1311 uncertainty of saturation pressure is found to be
 1312 increasing as the pressure drops. The cause of
 1313 the large uncertainty is due to the scattering of
 1314 the deviations between the estimated and mea-
 1315 sured pressure at low pressure levels as shown
 1316 in Fig. 7.

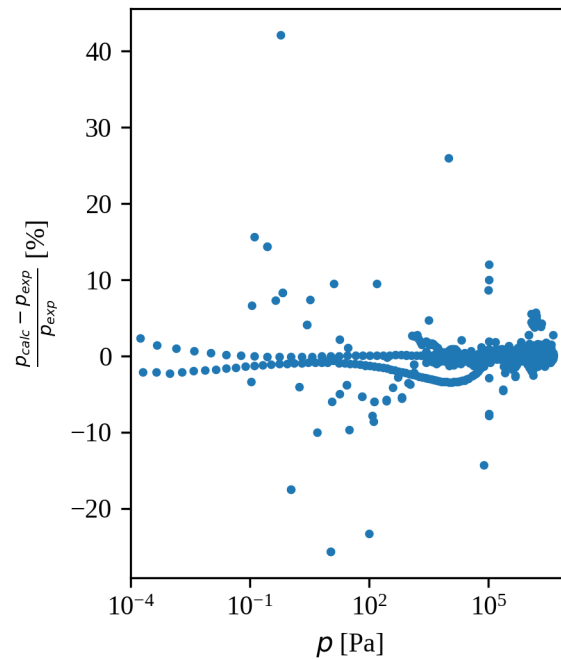


Figure 7: Relative deviations of pressure estimates

1317 As the pressure drops, the relative deviations
 1318 between the estimated and measured pressure
 1319 scatter. At high pressure, the relative devi-
 1320 ations concentrate between +10% and -10%.
 1321 However, as lower pressure, the distribution of
 1322 the relative deviations widens to between +40
 1323 % and -30 %. The large scattering of the rela-
 1324 tive deviation of saturation pressure at low lev-
 1325 els results in the increase of relative uncertain-
 1326 ties of saturation pressure with a drop of pres-
 1327 sure.

1328 To have a more comprehensive understand-
 1329 ing, the relative uncertainty of pressure in the
 1330 single phase region is also studied by plot-
 1331 ting the contour plot of its relative uncer-
 1332 tainty over a temperature-specific-volume (T -
 1333 $1/\rho$) plot. The contour plot is shown in Fig. 8.

Figure 8 shows that the relative uncertainties

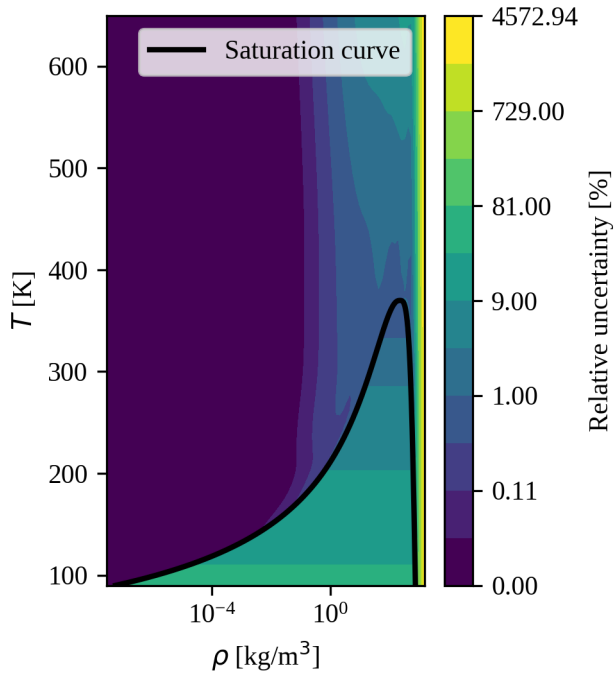


Figure 8: Relative uncertainty of pressure in a $T-1/\rho$ diagram

of pressure of vapor in the single-phase region are much less than the relative uncertainties of saturation pressure. There are some relative uncertainties of pressure of subcooled liquid at high densities that are high, but it fits the general understanding that the derivative of pressure with density is high in that regime and hence the relative uncertainty of pressure in the regime is high.

4.4 Uncertainty of properties in the single-phase region

To further understand how the uncertainties of EOS change in the single-phase region, the relative uncertainties of speed of sound, isochoric specific heat capacity, isobaric specific heat capacity and density are calculated at different temperature and pressure state points, and the results are shown in Figs. 9a to 9d.

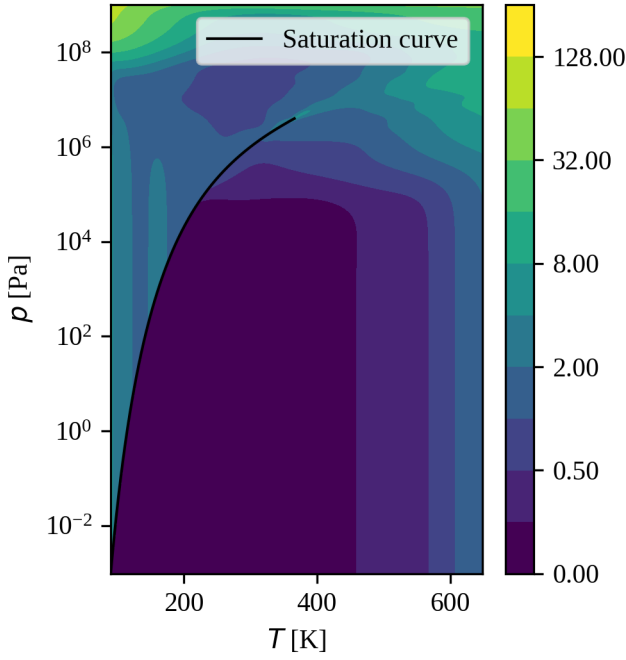
Figure 9a shows that the relative uncertainty of speed of sound is lower than 4 % in most cases except conditions near the critical point and at pressure higher than 10^8 Pa. At pressure higher than 10^8 Pa, only speed of sound data were only collected near 240 K and density data were collected between 370 K and 610 K. Other

property data were not collected in the pressure regime. Thus the figure only shows an uncertainty value lower than 8% between 240 K and 610 K at pressure higher than 10^8 Pa, and the uncertainty of the speed of sound remains high at all other temperature values in the pressure regime.

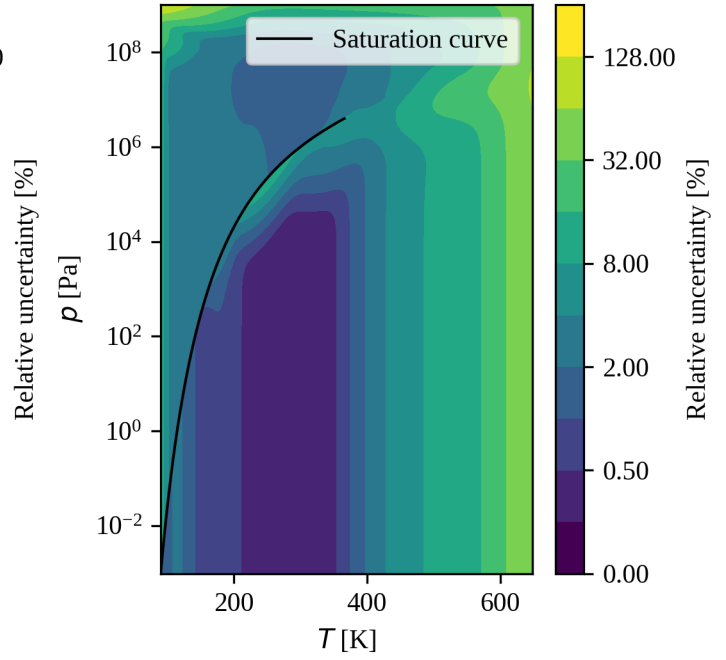
Figures 9b and 9c show a similar pattern in which the relative uncertainty remains lower than 4 % in the subcooled liquid region and highly superheated vapor region. However, the relative uncertainties of the specific heat are much more significant near the the saturated vapor line at 250 K. While the c_p and c_v of superheated vapor near the saturated curve at low temperatures should behave as an ideal gas, the relative uncertainties of c_p and c_v near the saturated curve at around 250 K are much higher than one of their ideal gas counterparts at lower pressure. While this may be caused by the approximation to use model deviation instead of measurement uncertainty to conduct the calculation, it may also caused by potential overfitting issues in the part of the EOS related to the residual Helmholtz energy.

Overfitting arises when a regression equation contains too many coefficients and is fit for the random variation in the experimental data rather than the systematic relationship between variables. Equations with overfitting issues usually result in very accurate prediction at the experimental data points but large model uncertainties.³⁹ Since c_p and c_v in the vapor phase with the exception of ones near the critical point should not differ too much from their ideal gas counterparts and the EOS part of the ideal gas contribution (α^0 in Eq. (14)) is not complex enough to result in significant overfitting, the large uncertainty is likely caused by the overfitting of the residual part of the Helmholtz energy arising from the intermolecular forces (α^r in Eq. (14)). To mitigate these issues and the uncertainties, simplification of EOS or constraints to the coefficients such as penalization should be made to reduce these unexpectedly high uncertainties.⁴⁰

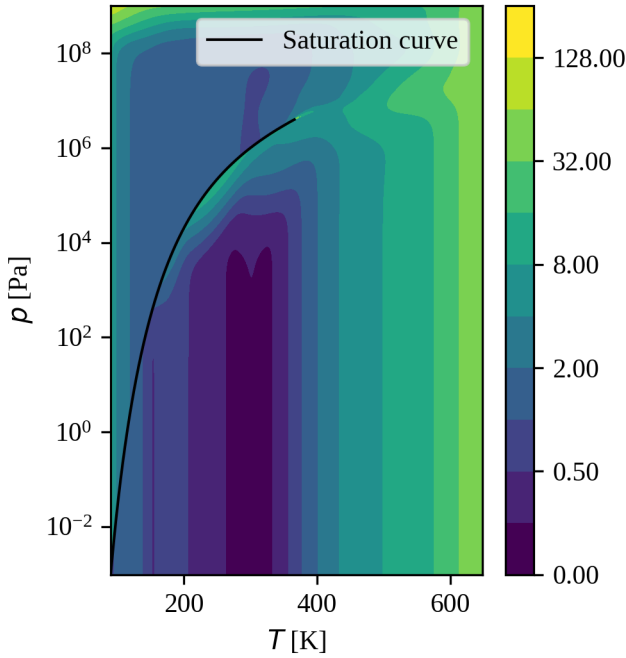
Figure 9d shows a different pattern. Relative uncertainty of density is lower than 0.25 % for all subcooled liquid states and is lower than



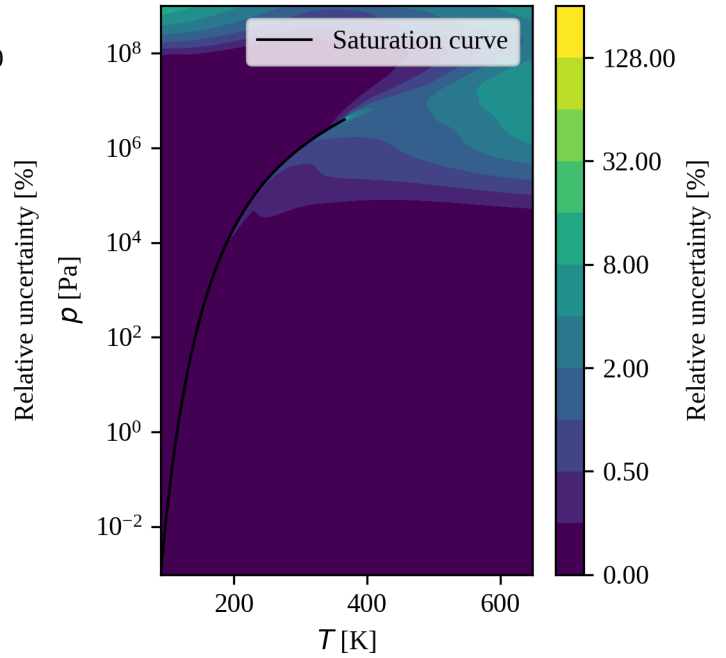
(a) Relative uncertainty of speed of sound



(b) Relative uncertainty of c_v



(c) Relative uncertainty of c_p



(d) Relative uncertainty of density

Figure 9: Relative uncertainties in p - T coordinates

1409 1 % for most highly superheated vapor states.¹⁴¹⁶
 1410 The relative uncertainty of density of the su-¹⁴¹⁷
 1411 perheated vapor at higher pressures also ranges¹⁴¹⁸
 1412 between 1 % and 4 %. The relative uncertainty¹⁴¹⁹
 1413 only exceeds 8 % in the critical region.¹⁴²⁰

1414 In summary, the relative uncertainties of EOS¹⁴²¹
 1415 are in general large in the critical region. For¹⁴²²

pressure and speed of sound, their relative un-
 certainties in the subcooled liquid region are
 higher than that of the superheated vapor re-
 gion. For specific heat capacities and densities,
 the relative uncertainties of superheated vapor
 close to saturation are higher than those of the
 subcooled liquid and more highly superheated

1423 vapor. 1468

1469

1470

1471

1472

1473

1474

1475

1476

1477

1478

1479

1480

1481

1482

1483

1484

1485

1486

1487

1488

1489

1490

1491

1492

1493

1494

1495

1496

1497

1498

1499

1500

1501

1502

1503

1504

1505

1506

1507

1508

1509

1510

1511

1512

1513

5 Conclusion

In this paper, a method to calculate the uncertainty of thermodynamic properties of Helmholtz-energy-explicit EOS is developed based on the parameter covariance matrix of nonlinear regression models. The covariance matrix can be calculated from the experimental data in the literature and the Jacobian matrix of the EOS with respect to the parameters of the EOS. To ensure that the effects of the Maxwell criteria and uncertainties of the differences of properties such as enthalpy values are properly calculated, the uncertainty calculation method also involves the linearization of the EOS and the covariance of the differences of properties.

To test the applicability and validity of the calculation method, it is demonstrated by a calculation of the uncertainties of the EOS of propane. The method also enables an analysis of the parameter correlation matrix which shows how the parameters are correlated with each other. It also demonstrates how the use of the Maxwell criteria and the rapid change of properties with respect to the state of the substances around their critical point result in larger uncertainties of properties along the superheated vapor line than the uncertainties of properties in the single-phase region. The results of this study allow users to take into account the uncertainties of the EOS in process model simulations. However, the results also show some limitations of the method:

- The uncertainty analysis does not present the effect of experimental uncertainty of the training data to the EOS because of the lack of information in some data sets of propane. The authors strongly encourage future research to take into account measurement uncertainties, if full and trustful measurement uncertainties have been obtained for each data point.
- The uncertainty analysis follows a linear propagation of error approach. This

method is the only computationally tractable method that could be used for a nonlinear model like the equation of state studied here. Other more advanced sampling techniques (Markov Chain Monte Carlo (MCMC) sampling methods, etc.) are too computationally expensive to be practically applied in technical applications.

- The method assumes a Gaussian distribution for the uncertainties of the EOS, and may fail to calculate the appropriate value at conditions which uncertainties distribute differently from the Gaussian distribution.
- The method assumes that all experimental data points are not correlated with each other. However, some training data points are not associated with comprehensive information on their measurement uncertainties and hence information on correlation between data, and more research is needed before the effect of correlation can be comprehensively accounted for by an uncertainty calculation method.
- The method does not involve the structural uncertainty in Table 1.
- The state-of-the-art fitting process of the EOS includes addition and removal of data points and constraints in an iterative fashion, and it is computationally expensive to involve the constantly changing and exact objective function for the fit of the EOS into the uncertainty calculation method. Thus the method has to use an approximated objective function of the EOS for the uncertainty calculation, and it is unknown how much error is introduced by the difference as a result.

Last but not least, it is recommended that users and developers of EOS perform this type of analysis in order to obtain insights about the uncertainties of the properties calculated by the EOS. Since the method does not incorporate other sources of uncertainties such as experimental uncertainties shown in Table 1, other

1514 methods to involve the experimental uncertain-1558
1515 ties should also be used to have a comprehensive1559
1516 understanding of uncertainties of EOS. 1560

1517 **Supporting Information.** Supporting In-1561
1518 formation is provided in three files. One file
1519 contains the mathematical derivation related to1562
1520 the differences of the expressions in this pa-1563
1521 per from that in some statistical textbooks,
1522 derivation for the Gibbs energy approximation1564
1523 in Fig. 1, the parameter identifiability analysis1566
1524 results, the Python code used to calculate the1567
1525 uncertainties of the thermodynamic properties1568
1526 of propane and the list of sources of experimen-1569
1527 tal data being used in the study. The covari-1570
1528 ance matrix is provided in `pcov.csv`, and the
1529 correlation matrix is provided in `pcor.csv`. 1572

1530 **Acknowledgement.** The authors would like
1531 to acknowledge Allan H. Harvey at National In-1573
1532 stitute of Standards and Technology, Boulder,1574
1533 CO, USA for his comments on the manuscript1575
1534 draft. Commercial equipment, instruments, or1576
1535 materials are identified only in order to ade-1577
1536 quately specify certain procedures. In no case1578
1537 does such identification imply recommendation1579
1538 or endorsement by the National Institute of
1539 Standards and Technology, nor does it imply1580
1540 that the products identified are necessarily the1581
1541 best available for the purpose. 1582
1583
1584

1542 References 1585

1543 (1) Frutiger, J.; Andreasen, J.; Liu, W.; Spli-1586
1544 ethoff, H.; Haglind, F.; Abildskov, J.;1587
1545 Sin, G. Working fluid selection for organic1588
1546 Rankine cycles – Impact of uncertainty of1589
1547 fluid properties. *Energy* **2016**, *109*, 987–1590
1548 997. 1591

1549 (2) Cheung, H.; Braun, J. E. A general1592
1550 method for calculating the uncertainty of1593
1551 virtual sensors for packaged air condition-1594
1552 ers. *Int. J. Refrig* **2016**, *63*, 225–236. 1595

1553 (3) Huang, G.; Wang, S.; Xu, X. A ro-1596
1554 bust model predictive control strategy1597
1555 for improving the control performance of1598
1556 air-conditioning systems. *Energy Convers.*1599
1557 *Manage.* **2009**, *50*, 2650–2658. 1600
1601

(4) Shan, K.; Wang, S.; Xiao, F.; Sun, Y. Sen-
sitivity and uncertainty analysis of cool-
ing water control strategies. *HVAC&R Re-
search* **2013**, *19*, 435–443.

(5) Reddy, T. A.; Niebur, D.; Ander-
sen, K. K.; Pericolo, P. P.; Cabrera, G.
Evaluation of the Suitability of Differ-
ent Chiller Performance Models for On-
Line Training Applied to Automated
Fault Detection and Diagnosis (RP-1139).
HVAC&R Research **2003**, *9*, 385–414.

(6) Proppe, J.; Reiher, M. Reliable estima-
tion of prediction uncertainty for physico-
chemical property models. *J. Chem. The-
ory Comput.* **2017**, *13*, 3297–3317.

(7) Hukkerikar, A.; Sarup, B.; Ten Kate, A.;
Abildskov, J.; Sin, G.; Gani, R. Group-
contribution+ (GC+) based estimation of
properties of pure components: Improved
property estimation and uncertainty anal-
ysis. *Fluid Phase Equilib.* **2012**, *321*, 25–
43.

(8) Morgan, J.; Bhattacharyya, D.; Tong, C.;
Miller, D. C. Uncertainty quantification of
property models: Methodology and its ap-
plication to CO₂-loaded aqueous MEA so-
lutions. *AIChE J.* **2017**, *61*, 1822–1839.

(9) Kamei, A.; Beyerlein, S. W.; Jacob-
sen, R. T. Application of nonlinear regres-
sion in the development of a wide range
formulation for HCFC-22. *Int. J. Thermo-
phys.* **1995**, *16*, 1155–1164.

(10) Wagner, W.; Pruß, A. The IAPWS For-
mulation 1995 for the Thermodynamic
Properties of Ordinary Water Substance
for General and Scientific Use. *J. Phys.
Chem. Ref. Data* **2002**, *31*, 387–535.

(11) Lemmon, E. W.; Jacobsen, R. T. Equa-
tions of State for Mixtures of R-32, R-
125, R-134a, R-143a, and R-152a. *J. Phys.
Chem. Ref. Data* **2004**, *33*, 593.

(12) Lemmon, E. W.; McLinden, M. O.; Wag-
ner, W. Thermodynamic Properties of
Propane. III. A Reference Equation of

- 1602 State for Temperatures from the Melt-¹⁶⁴³
1603 ing Line to 650 K and Pressures up to¹⁶⁴⁴
1604 1000 MPa. *J. Chem. Eng. Data* **2009**, *54*,¹⁶⁴⁵
1605 3141–3180. ¹⁶⁴⁶
¹⁶⁴⁷
- 1606 (13) Lemmon, E. W. Pseudo-Pure Fluid Equa-
1607 tions of State for the Refrigerant Blends¹⁶⁴⁸
1608 R-410A, R-404A, R-507A, and R-407C.¹⁶⁴⁹
1609 *Int. J. Thermophys.* **2003**, *24*, 991–1006. ¹⁶⁵⁰
¹⁶⁵¹
- 1610 (14) Cheung, H.; Bach, C. K. Prediction of
1611 uncertainty of 10-coefficient compressor¹⁶⁵²
1612 maps for extreme operating conditions.¹⁶⁵³
1613 IOP Conference Series: Materials Science
1614 and Engineering. 2015; p 012078. ¹⁶⁵⁴
¹⁶⁵⁵
- 1615 (15) ASME, *ASME PTC 19.1-2013 Test Un-*¹⁶⁵⁶
1616 *certainty Performance Test Codes*; The
1617 American Society of Mechanical Engi-¹⁶⁵⁸
1618 neers: New York, 2013. ¹⁶⁵⁹
¹⁶⁶⁰
- 1619 (16) JCGM, *JCGM 100:2008 Evaluation of*¹⁶⁶¹
1620 *measurement data — Guide to the expres-*¹⁶⁶²
1621 *sion of uncertainty in measurement*; Joint
1622 Committee for Guides in Metrology, 2008.¹⁶⁶³
¹⁶⁶⁴
- 1623 (17) ASME, *ASME V&V 10-2006 Guide for*¹⁶⁶⁵
1624 *Verification and Validation in Computa-*¹⁶⁶⁶
1625 *tional Solid Mechanics*; American Society¹⁶⁶⁷
1626 of Mechanical Engineers: New York, 2006.
¹⁶⁶⁸
- 1627 (18) Cheung, H.; Wang, S. A comparison of¹⁶⁶⁹
1628 the effect of empirical and physical mod-¹⁶⁷⁰
1629 eling approaches to extrapolation capabil-
1630 ity of compressor models by uncertainty¹⁶⁷¹
1631 analysis: A case study with common semi-¹⁶⁷²
1632 empirical compressor mass flow rate mod-¹⁶⁷³
1633 els. *Int. J. Refrig* **2018**, *86*, 331–343. ¹⁶⁷⁴
¹⁶⁷⁵
- 1634 (19) Feistel, R.; Lovell-Smith, J. W.; Saun-¹⁶⁷⁶
1635 ders, P.; Seitz, S. Uncertainty of empirical
1636 correlation equations. *Metrologia* **2016**,¹⁶⁷⁷
1637 *53*, 1079. ¹⁶⁷⁸
¹⁶⁷⁹
- 1638 (20) Lovell-Smith, J. W.; Saunders, P.; Feis-¹⁶⁸⁰
1639 tel, R. Unleashing Empirical Equations¹⁶⁸¹
1640 with “Nonlinear Fitting” and “GUM Tree¹⁶⁸²
1641 Calculator”. *Int. J. Thermophys.* **2017**,¹⁶⁸³
1642 *38*, 148. ¹⁶⁸⁴
¹⁶⁸⁵
¹⁶⁸⁶
- (21) Frutiger, J.; Bell, I.; O’Connell, J. P.;
Kroenlein, K.; Abildskov, J.; Sin, G. Un-
certainty assessment of equations of state
with application to an organic Rankine cy-
cle. *Mol. Phys.* **2017**, *115*, 1225–1244.
- (22) Lötgering-Lin, O.; Schöniger, A.;
Nowak, W.; Gross, J. Bayesian Model
Selection Helps To Choose Objectively
between Thermodynamic Models: A
Demonstration of Selecting a Viscosity
Model Based on Entropy Scaling. *Ind.*
Eng. Chem. Res. **2016**, *55*, 10191–10207.
- (23) Kline, S. J.; McClintock, F. A. Describ-
ing uncertainties in single-sample experi-
ments. *Mech. Eng.* **1953**, *75*, 3–8.
- (24) Sin, G.; Gernaey, K. V.; Lantz, A. E. Good
modeling practice for PAT applications:
Propagation of input uncertainty and sen-
sitivity analysis. *Biotechnol. Progr.* **2009**,
25, 1043–1053.
- (25) Dong, Q.; Chirico, R. D.; Yan, X.;
Hong, X.; Frenkel, M. Uncertainty Re-
porting for Experimental Thermodynamic
Properties. *J. Chem. Eng. Data* **2005**, *50*,
546–550.
- (26) Seber, G.; Wild, C. J. *Nonlinear regres-*
sion; John Wiley & Sons, Inc.: Hoboken,
NJ, USA, 1989.
- (27) Sin, G.; Gernaey, K. V.; Neumann, M. B.;
van Loosdrecht, M. C. M.; Gujer, W.
Global sensitivity analysis in wastewa-
ter treatment plant model applications:
Prioritizing sources of uncertainty. *Water*
Res. **2011**, *45*, 639–651.
- (28) Frutiger, J.; Marcarie, C.; Abildskov, J.;
Sin, G. A Comprehensive Methodology for
Development, Parameter Estimation, and
Uncertainty Analysis of Group Contribu-
tion Based Property Models—An Applica-
tion to the Heat of Combustion. *J. Chem.*
Eng. Data **2016**, *61*, 602–613.
- (29) Çengel, Y. A.; Boles, M. A. *Thermody-*
namics: An Engineering Approach, 5th
ed.; McGraw-Hill: Boston, 2005.

- 1687 (30) Span, R. *Multiparameter Equations of State - An Accurate Source of Thermodynamic Property Data*; Springer, 2000. 1731
- 1688
- 1689
- 1690 (31) Tillner-Roth, R.; Baehr, H. D. A International Standard Formulation for the Thermodynamic Properties of 1,1,1,2-Tetrafluoroethane (HFC-134a) for Temperatures from 170 K to 455 K and Pressures up to 70 MPa. *J. Phys. Chem. Ref. Data* **1994**, *23*, 657–729. 1735
1736
1737
1738
1739
1740
- 1697 (32) Bell, I. H.; Satyro, M.; Lemmon, E. W. Consistent Two Parameters for More than 2500 Pure Fluids from Critically Evaluated Experimental Data. *J. Chem. Eng. Data* **2018**, *63*, 2402–2409. 1741
1742
1743
1744
1745
- 1702 (33) Coleman, H. W.; Steele, W. G. *Experimentation, Validation, and Uncertainty Analysis for Engineers*, 3rd ed.; Wiley: Hoboken, N.J, 2009. 1746
1747
1748
1749
- 1706 (34) Thorade, M.; Saadat, A. Partial derivatives of thermodynamic state properties for dynamic simulation. *Env. Earth Sci.* **2013**, *70*, 3497–3503. 1707
1708
1709
- 1710 (35) Diky, V.; Chirico, R. D.; Muzny, C. D.; Kazakov, A. F.; Kroenlein, K.; Magee, J. W.; Abdulagatov, I.; Kang, J. W.; Frenkel, M. ThermoData Engine (TDE) software implementation of the dynamic data evaluation concept. 7. Ternary mixtures. *J. Chem. Inf. Model.* **2011**, *52*, 260–276. 1711
1712
1713
1714
1715
1716
1717
- 1718 (36) Frenkel, M.; Chirico, R. D.; Diky, V.; Yan, X.; Dong, Q.; Muzny, C. ThermoData Engine (TDE): Software Implementation of the Dynamic Data Evaluation Concept. *J. Chem. Inf. Model.* **2005**, *45*, 816–838. 1719
1720
1721
1722
1723
- 1724 (37) Diky, V.; Chirico, R. D.; Muzny, C. D.; Kazakov, A. F.; Kroenlein, K.; Magee, J. W.; Abdulagatov, I.; Kang, J. W.; Gani, R.; Frenkel, M. ThermoData Engine (TDE): Software implementation of the dynamic data evaluation concept. 8. Properties of material streams and solvent design. *J. Chem. Inf. Model.* **2012**, *53*, 249–266. 1732
1733
1734
1735
1736
1737
1738
1739
1740
- (38) Diky, V.; Chirico, R. D.; Muzny, C. D.; Kazakov, A. F.; Kroenlein, K.; Magee, J. W.; Abdulagatov, I.; Frenkel, M. ThermoData Engine (TDE): Software implementation of the dynamic data evaluation concept. 9. Extensible thermodynamic constraints for pure compounds and new model developments. *J. Chem. Inf. Model.* **2013**, *53*, 3418–3430. 1741
1742
1743
1744
1745
- (39) Hawkins, D. M. The Problem of Overfitting. *J. Chem. Inf. Comput. Sci.* **2004**, *44*, 1–12. 1746
1747
1748
1749
- (40) Babyak, M. A. What You See May Not Be What You Get: A Brief, Nontechnical Introduction to Overfitting in Regression-Type Models. *Psychosom. Med.* **2004**, *66*, 411–421. 1750
1751
1752
1753